**Figure 1. Co-localization of HBcAg and HBsAg with AGO2 in stably transfected T23 cells.** A) Anti-AGO2 and anti-HBc staining overlapped in stably transfected T23 cells, but not in HepG2 control cells, suggesting an interaction between HBc and AGO2. B) HBc-AGO2 was detected in T23 but not HepG2 cells using proximity ligation assays (PLA), suggesting a protein-protein interaction between HBcAg and AGO2. C) Overlap of anti-AGO2 and anti-HBs staining suggests co-localization of HBs and AGO2. D) Anti- HBc, and anti-HBs staining overlapped in T23 cells, which may indicate that HBc and HBs co-localize. E) Overlap of anti-AGO2, anti-HBc, and anti-HBs staining in T23 cells suggests that all three proteins may co-localize.
doi:10.1371/journal.pone.0047490.g001

## Pathway Analysis

Predicted gene targets of up-regulated miRNAs were most strongly associated with the GO term PROTEIN_TYROSINE_PHOSPHATASE_ACTIVITY (P = 5.24E−3), and down-regulated miRNAs were associated with the term POSITIVE_REGULATION_OF_JNK_ACTIVITY (P 9.47e−4). Predicted target genes associated with phosphatase activity and dephosphorylation included MTMR3, PTPN18, DUSP5, PTPN2, DUSP2, and PPP1CA.

## MiRNA Expression in Liver Biopsy Samples

We compared miRNA expression in non-cancerous liver biopsy samples from a patient with chronic HBV to two uninfected patients (Table S2, Fig. S8). MiRNA levels were highly correlated between liver tissue and serum in all patients (P = <0.001; $R^2 = 0.57$), including the top HBV-associated miRNAs identified by microarray and RT-PCR analysis in this study.

## Co-localization of HBcAg and HBsAg with AGO2

Using immunocytochemistry and PLA analysis, we found that HBV core protein and AGO2 co-localized within T23 cells (Fig. 1A–B), suggesting a potential protein-protein interaction between HBcAg and AGO2. AGO2 also co-localized with HBs in T23 cells (Fig. 1C), indicating a potential interaction between HBs and AGO2. Overlap between anti-HBc and anti-HBs staining (Fig. 1D) and between anti-AGO2, anti-HBc, and anti-HBs (Fig. 1E) suggests that these three proteins may co-localize. No overlap was observed between anti-AGO2 and anti-HBx staining in HepG2 cells transfected with HBx expression plasmid (p3FLAG-HBx) nor in control cells, suggesting that HBx does not interact with AGO2 (data not shown).

## Subcellular Localization

We also examined HBcAg sub-cellular localization using immunocytochemistry and PLA analysis and found that HBcAg localized to several intracellular compartments, including the ER, autophagosomes, endosomes, and Golgi (Fig. 2). No evidence was found for interaction with mitochondria (data not shown). Using immunocytochemistry, HBsAg was also found to localize diffusely to several intracellular compartments, including the ER, endosomes, autophagosomes, Golgi, mitochondria, processing bodies, multi-vesicular bodies, and the nuclear envelope (Fig. 3). HBx localized non-specifically in the nucleus and cytoplasm, and no sub-cellular location could be ascertained (Fig. S9).

## RNA Interference against AGO2

Antisense RNA directed against AGO2 strongly suppressed AGO2 expression (Fig. 4A) and resulted in lower HBV DNA (Fig. 4B) and HBsAg (Fig. 4C) levels in the supernatant. Cell viability was not significantly reduced (Fig. 4D).

# Discussion

In this study, we report a set of miRNAs that were up-regulated in serum of HBV infected individuals compared to healthy

**Table 3.** Quantitative RT-PCR results of selected miRNAs associated in serum of chronic HBV patients.

| Factor | Total (n = 270) | HBV (n = 248) | Healthy (n = 22) | P |
|---|---|---|---|---|
| hsa-miR-122/cel-miR-238 | 0.1513 (0.0068–2.5) | 0.1635 (0.0068–2.5) | 0.02074 (0.013–0.04) | 1.19E−13 |
| hsa-miR-22/cel-miR-238 | 0.3 (0.06–1.7) | 0.3028 (0.06–1.7) | 0.2252 (0.11–0.48) | 6.35E−03 |
| hsa-miR-99a/cel-miR-238 | 0.09121 (0.0046–2.4) | 0.102 (0.0086–2.4) | 0.0136 (0.0046–0.051) | 4.61E−12 |
| hsa-miR-720/cel-miR-238 | 0.1206 (0.024–3.7) | 0.1345 (0.031–3.7) | 0.04274 (0.024–0.12) | 8.93E−11 |
| hsa-miR-125b/cel-miR-238 | 0.09732 (0.0066–3.1) | 0.1131 (0.0066–3.1) | 0.02255 (0.0066–0.05) | 1.92E−11 |
| hsa-miR-1275/cel-miR-238 | 0.4842 (0.099–1.6) | 0.5046 (0.099–1.6) | 0.4044 (0.24–0.6) | 0.010781066 |
| hsa-miR-1826/cel-miR-238 | 0.5023 (0.14–4.6) | 0.5583 (0.26–4.6) | 0.33 (0.14–1.4) | 7.23E−03 |
| hsa-miR-1308/cel-miR-238 | 2.831 (1.1–6.9) | 2.578 (1.1–6.9) | 3.113 (2.3–4.7) | 0.223164946 |
| hsa-miR-923/cel-miR-238 | 3.8 (1.8–9.6) | 4.141 (1.8–9.6) | 3.01 (2–5) | 0.104331611 |
| hsa-miR-1280/cel-miR-238 | 1.089 (0.36–5) | 1.332 (0.6–5) | 0.5275 (0.36–0.8) | 1.06E−05 |
| hsa-miR-26a/cel-miR-238 | 1.221 (0.34–3.4) | 1.221 (0.34–3.4) | 1.231 (0.82–2.4) | 0.532171224 |
| hsa-let-7a/cel-miR-238 | 0.9608 (0.2–2.5) | 0.9211 (0.2–2.5) | 1.074 (0.71–1.9) | 0.235258945 |
| hsa-let-7f/cel-miR-238 | 1.134 (0.052–2.6) | 1.126 (0.052–2.6) | 1.143 (0.8–1.7) | 0.639411853 |
| hsa-let-7d/cel-miR-238 | 1.147 (0.35–1.9) | 1.106 (0.35–1.8) | 1.231 (0.73–1.9) | 2.88E−01 |
| hsa-miR-638/cel-miR-238 | 1.23 (0.3–7) | 1.082 (0.3–7) | 1.366 (0.68–4) | 0.288244047 |
| hsa-miR-1908/cel-miR-238 | 1.369 (0.45–3.2) | 1.357 (0.45–1.9) | 1.447 (0.7–3.2) | 0.370765019 |
| hsa-miR-34a/cel-miR-238 | 0.07502 (0.013–1.2) | 0.108 (0.026–1.2) | 0.02738 (0.013–0.044) | 1.41E−05 |
| hsa-miR-886-5p/cel-miR-238 | 1.627 (0.54–3.6) | 1.773 (0.54–3.6) | 1.55 (0.97–2.7) | 0.478520977 |

Expression levels were compared using the Mann-Whitney U test.
doi:10.1371/journal.pone.0047490.t003

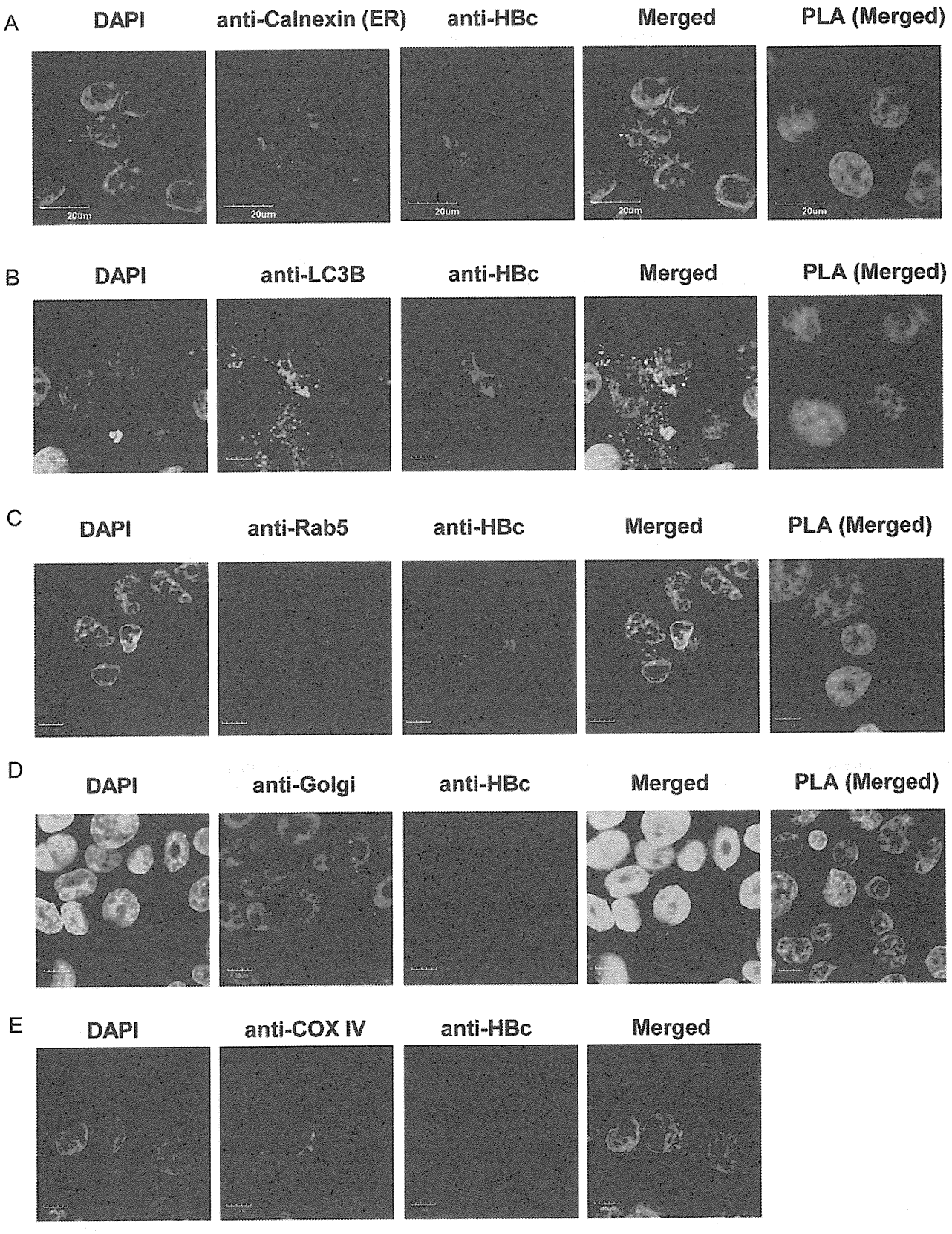


**Figure 2. Interactions between HBc and HBs.** A) Co-localization of anti-HBc and anti-Calnexin staining by immunocytochemistry and PLA analysis indicate that HBc probably localizes in the ER. Overlap with B) anti-LC3B, C) anti-Rab5, and D) anti-Golgi staining suggests that HBc probably also localizes in autophagosomes, endosomes, and Golgi, respectively. E) However, no overlap was observed with anti-COX IV staining, indicating that HBc probably does not localize at mitochondria.
doi:10.1371/journal.pone.0047490.g002

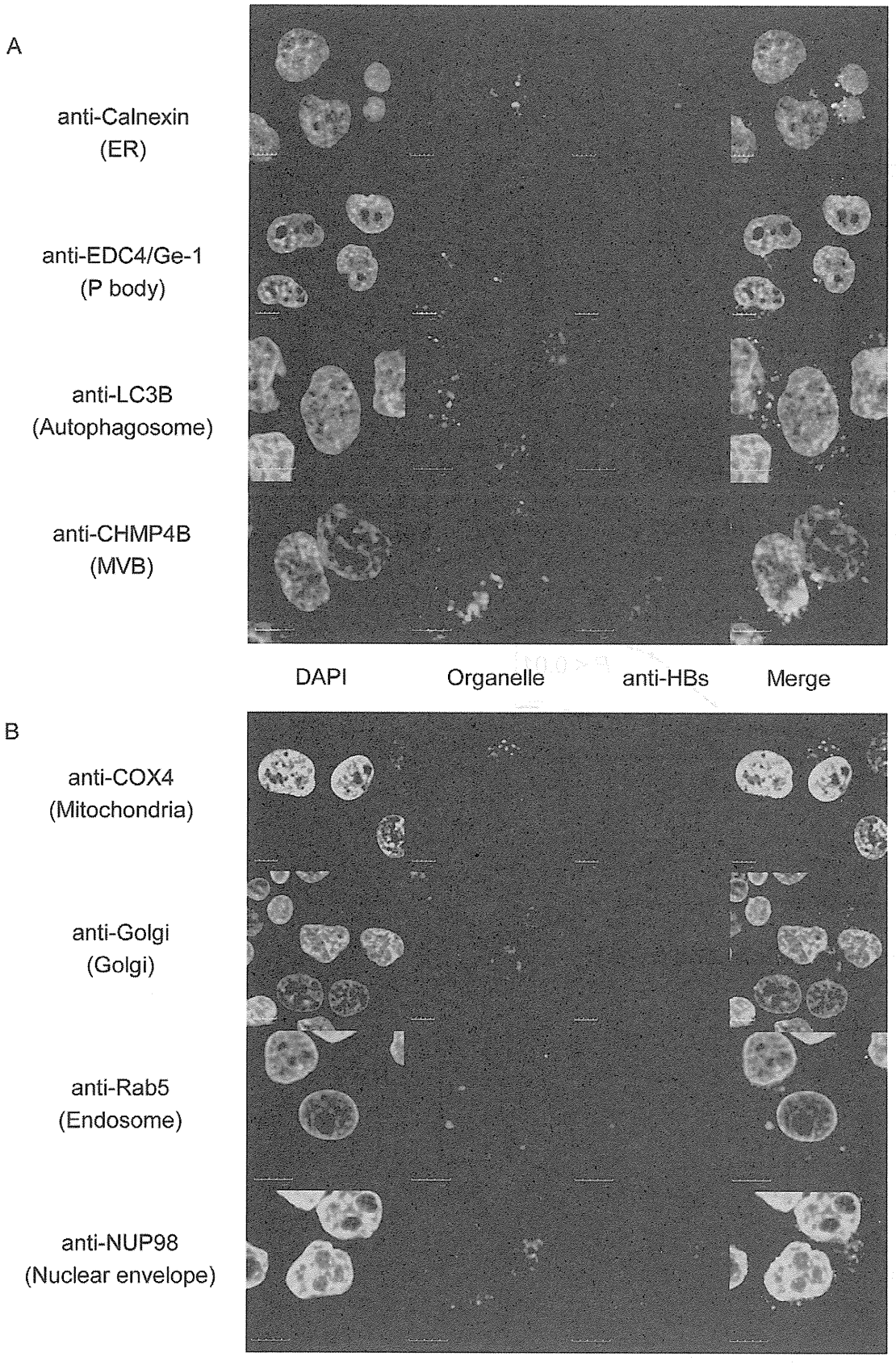


**Figure 3. HBsAg localization.** A) Co-localization of anti-HBs suggests that HBs localizes in the ER, processing bodies, autophagosomes, and multivesicular bodies, B) and more diffusely in mitochondria, Golgi, endosomes, and at the nuclear envelope.
doi:10.1371/journal.pone.0047490.g003

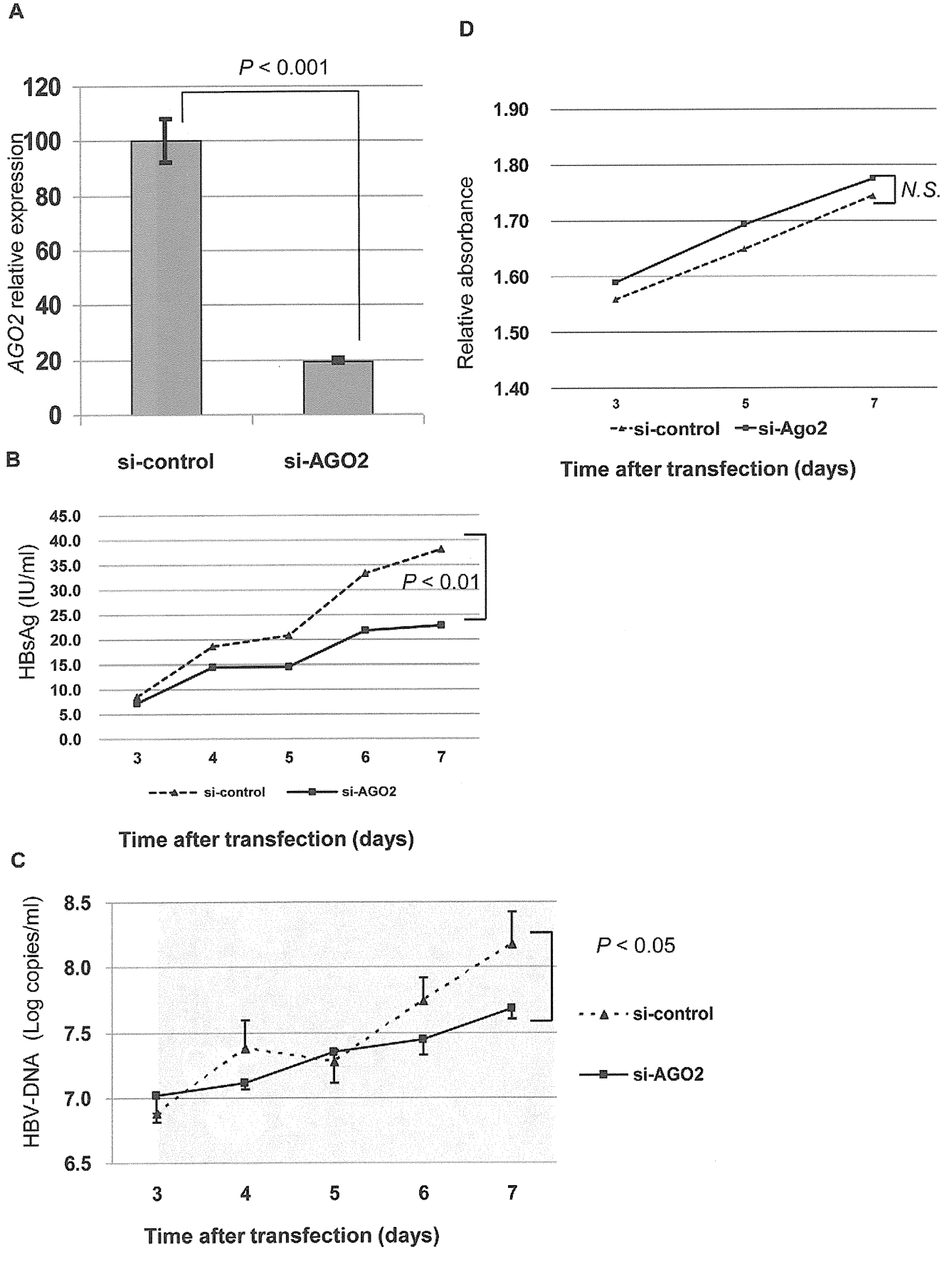
A
P < 0.001
AGO2 relative expression
120
100
80
60
40
20
0
si-control
si-AGO2
D
Relative absorbance
1.90
1.80
1.70
1.60
1.50
1.40
N.S.
3
5
7
si-control
si-Ago2
Time after transfection (days)
B
HBsAg (IU/ml)
45.0
40.0
35.0
30.0
25.0
20.0
15.0
10.0
5.0
0.0
P < 0.01
3
4
5
6
7
si-control
si-AGO2
Time after transfection (days)
C
HBV-DNA (Log copies/ml)
8.5
8.0
7.5
7.0
6.5
P < 0.05
si-control
si-AGO2
3
4
5
6
7
Time after transfection (days)

**Figure 4. siRNA knock down of AGO2 expression.** A) Knock down of *AGO2* expression in T23 cells by specific siRNAs for *AGO2* or control siRNAs, confirmed by real-time quantitative RT-PCR analysis. B) Supernatant HBs antigen, and C) HBV-DNA were measured. Both were higher in supernatant of cells transfected with si-control than in cells transfected with si-*AGO2*. D) There was no significant difference in cell viability between cells transfected with si-control compared to those with si-*AGO2*.
doi:10.1371/journal.pone.0047490.g004

controls. Mir-122, miR-22, miR-99a, and miR-125b in particular, were significantly elevated in serum of HBV patients. We also showed that AGO2, an essential component of the RNA silencing complex, co-localizes with both HBc and HBs proteins. HBc and/or HBs localize to several organelles associated with protein synthesis, processing, and degradation, including the ER, Golgi, endosomes, autophagosomes, processing bodies, and multivesicular bodies. Although we expected that depletion of AGO2 would relieve inhibition of HBV replication, we found instead that knockdown of AGO2 appears to inhibit HBV replication, implying that HBV may require AGO2 during its life cycle.

The role of AGO2 is unclear, but viruses have previously been shown to interfere with elements of the RNA-induced gene silencing pathway [17]. HCV core protein and the HIV-1 Tat protein suppress gene silencing by inhibiting Dicer, a cytoplasmic protein that processes pre-microRNA [18]. HBV down-regulates expression of Drosha, the nuclear protein involved in the first step of miRNA processing, which might globally suppress miRNA expression levels [19]. Viruses also influence expression of individual miRNAs [17].

Considering that miR-122 strongly suppresses HBV replication, it is curious that HBV is nonetheless often able to establish chronic infection in the liver [20,21,22]. In the case of HCV, miR-122/AGO2 binding stabilizes the HCV genome and prevents degradation, such that suppression of either miR-122 or AGO2 inhibits HCV replication [23,24,25]. In HBV, we also found that AGO2 knockdown suppresses replication, but Wang et al. demonstrated that anti-sense depletion of miR-122 promoted HBV replication instead of suppressing it [26]. MiR-122 suppresses HBV replication both through direct binding to HBV RNA as well as indirectly through cyclin G1-modulated p53 activity [20,27,28]. HBV might therefore be expected to down-regulate miR-122 levels to evade miR-122 binding and suppression. Wang et al. indeed found that miR-122 levels are significantly decreased in the liver of chronic HBV patient [26], whereas elevated miR-122 levels in the serum have been reported [4,29].

One explanation for the discrepancy between liver and serum miR-122 levels might be that HBV sequesters and expels AGO2-bound miR-122 inside of HBsAg particles, possibly along with other miRNAs that interfere with the viral life cycle. HBV vastly over-produces surface proteins that self-assemble into what were initially thought to be empty particles [30,31], but which may contain miRNAs stably bound to AGO2 [5]. Although HBV is a DNA virus, it relies on reverse transcription via an RNA intermediate in a way similar to retroviruses. Bouttier et al. showed that two unrelated retroviruses, HIV-1 and PFV-1, both require AGO2 interaction with viral RNA for assembly of viral particles. In these viruses, AGO2 is recruited to viral RNA and encapsidated along with it without impairing translation of viral RNA [32]. This suggests that some viruses may take advantage of another function of Argonaute, such as its role in the formation of P-bodies [33], although AGO2 possesses intrinsic exonuclease activity that must be countered. AGO2-mediated gene silencing requires recruitment of GW182 via multiple GW-rich regions [34]. While HIV-1 and PFV-1 encapsidate AGO2, they do not encapsidate GW182, which might provide a means to suppress AGO2 silencing. Some plant viruses use molecular mimicry to inhibit RISC activity by binding to Argonaute proteins through virally encoded WG/GW motifs [35]. Although HBV proteins appear to lack WG/GW motifs, the HBV core protein may use a similar mechanism to disrupt RISC activity while preserving other AGO2 functions. One possibility involves HSP90, a chaperone involved in maintenance of the polymerase/pgRNA complex. HSP90 binds to HBV core protein dimers and is internalized in capsids, but it also binds to the N-terminus of AGO2 and may be required for miRNA loading and targeting to P-bodies [36,37]. Co-localization studies with other proteins and analysis of bound miRNAs may be necessary to elucidate the role of AGO2 in HBV replication, but we speculate that HBV proteins might suppress miRNA activity by binding to and sequestering AGO2 and their bound miRNAs.

Pathway analysis of the predicted targets of the up-regulated serum miRNAs in HBV patients showed that genes involved in phosphatase activity were significantly over-represented. Each of several miRNAs, including miR-122, miR-125b, and miR-99a, was predicted to target a different phosphorylation-associated gene. Regulation of phosphorylation appears to be important in HBV replication, as phosphorylation of the C terminal domain of the HBV core protein is essential for pgRNA packaging and HBV capsid maturation [38]. Phosphorylation also inhibits AGO2 binding of miRNA [39] and is involved in localization to P-bodies [40]. Recent studies have demonstrated that HBV enhances and exploits autophagy via the HBx and small HBs proteins to promote viral DNA replication and envelopment without increasing the rate of protein degradation [41,42]. Sir et al suggested that autophagy may affect dephosphorylation and maturation of the core protein, which protects viral DNA during replication [43]. These reports suggest that HBV exploits multiple cellular pathways in order to establish an intracellular environment conducive to replication.

Although many HBV-associated miRNAs have been reported, the functions of only a few have been examined. MiR-122, miR-125a-5p, miR-199a-3p and miRNA-210 have all been reported to bind to and directly suppress HBV RNA [8,27,44], whereas other miRNAs have been shown to promote or suppress HBV replication indirectly. MiR-1 enhances HBV core promoter activity by up-regulating FXR$\alpha$, a transcription factor essential for HBV replication [45], whereas miR-141 suppresses HBsAg production in HepG2 cells by down-regulating promoter activity via PPARA [46]. The role of miR-22 and miR-99a in HBV infection is less clear, but both are involved in regulation of cell fate and are implicated in development of HCC. MiR-99a is one of the most highly expressed miRNAs in normal liver tissue and is severely down-regulated in HCC and other cancers, suggesting a role as a tumor suppressor [47]. MiR-99a alters sensitivity to TGF-$\beta$ activity by suppressing phosphorylation of SMAD3 [48], whereas the HBx protein disrupts TGF-$\beta$ signaling by shifting from the pSmad3C pathway to the oncogenic pSmad3L pathway [49]. MiR-22 acts as a tumor suppressor by inducing cellular senescence and is down-regulated in several cancer lines [50]. However, over-expression of miR-22 in males is associated with down-regulation of ER$\alpha$ expression, which compromises the protective effect of estrogen and leads to up-regulation of IL-1$\alpha$ in hepatocytes under stress caused by reactive oxygen species, which is another hallmark of HBx interference [51]. Differences in

miRNA levels between hepatic and serum miRNA profiles may reveal miRNAs that play an essential role in the HBV life cycle, with potential application to miRNA-based diagnosis and therapy.

In this study we demonstrated potential interactions between AGO2 and HBc and HBs, but not HBx, in stably transfected HepG2 cells. Suppression of HBV DNA and HBsAg in the supernatant following AGO2 knockdown and the presence of HBV-associated miRNAs in the serum may indicate a dependency on AGO2 during the HBV life cycle.

## Supporting Information

**Figure S1 Heat map of miRNA expression.** Healthy controls and patients with chronic HBV clustered separately based on serum miRNA expression. "Healthy males" and "healthy females" refer to serum mixtures of 12 uninfected males and 10 uninfected females, respectively. "HBV low" and "HBV high" refer to serum mixtures from 10 patients with low (≤42 IU/l) ALT levels and 10 patients with high ALT levels (>42 IU/l), respectively.
(TIF)

**Figure S2 Pairwise correlations among pooled serum miRNA samples.** Pooled serum samples were collected from 10 healthy males, 10 healthy females, 10 HBV patients with low ALT levels, and 10 HBV patients with high ALT levels. Pairwise correlations in miRNA expression levels among all four pooled samples were strong (>0.90; P<0.001), but correlations were strongest between the healthy male and female samples (0.98) and between the low and high ALT HBV patients (0.98), suggesting that expression of a subset of miRNAs is altered during HBV infection.
(TIF)

**Figure S3 Relationship between serum miRNAs and HBsAg levels in chronic HBV patients.** Serum levels of several miRNAs were significantly correlated with HBsAg levels in patients with chronic HBV. MiR-99a, miR-122, and miR-125b levels were most strongly correlated with HBsAg levels, with $R^2$ of 0.69, 0.56, and 0.54, respectively.
(TIF)

**Figure S4 Relationship between serum miRNAs and HBV DNA levels in chronic HBV patients.** Serum levels of several miRNAs were significantly correlated with HBV DNA levels in patients with chronic HBV. MiR-122, miR-99a, and miR-125b levels were most strongly correlated with HBV DNA levels, with $R^2$ of 0.44, 0.43, and 0.39, respectively.
(TIF)

**Figure S5 Relationship between serum miRNAs and ALT levels in chronic HBV patients.** Serum levels of several miRNAs were significantly but somewhat diffusely correlated with ALT levels in patients with chronic HBV. MiR-122 and miR-22 levels were correlated with ALT levels with $R^2$ of 0.25 and 0.21, respectively.
(TIF)

**Figure S6 Relationship between serum miRNAs and presence of HBe antigen in chronic HBV patients.** Serum levels of miR-122, miR-99a, miR-720, and miR-125b were significantly elevated in patients positive for the HBe antigen.
(TIF)

**Figure S7 Relationship between serum miRNAs and presence of HBe antibody in chronic HBV patients.** Serum levels of miR-122, miR-99a, miR-720, and miR-125b were significantly elevated in patients negative for the HBe antibody.
(TIF)

**Figure S8 Relationship between individual miRNAs in the liver and serum.** Each point represents the level of a specific miRNA in non-cancerous liver tissue relative to serum in the same patient. Red points represent miRNA levels from a patient with chronic HBV, and blue and green points correspond to two different uninfected control subjects. Large red points and labels indicate the subset of miRNAs (Tables 2 and 3) that were significantly elevated in serum of chronic HBV patients. MiRNA expression levels were positively correlated ($R^2 = 0.57$; P<2.1E-16) between liver tissue and serum, suggesting that serum levels broadly reflect miRNA levels in the liver. There appears to be no clear discrepancy between liver and serum miRNA levels in the HBV-infected patient compared to the two uninfected patients.
(TIF)

**Figure S9 Subcellular localization of HBx analyzed by immunocytochemistry.** HBx localized non-specifically in the nucleus and cytoplasm, but we were unable to verify the subcellular location. Anti-Rab5 staining for endosomes is shown for illustration, but results were similar using antibodies against other compartments.
(TIF)

**Table S1 Antibodies used for immunocytochemistry.**
(DOC)

**Table S2 Significantly up- or down-regulated miRNAs in liver samples from an HBV-infected patient compared to two non-HBV-infected patients.**
(DOC)

## Acknowledgments

This work was carried out at the Analysis Center of Life Science, Hiroshima University.

## Author Contributions

Conceived and designed the experiments: KC CNH SA MT DM HAB HO NH. Performed the experiments: MT DM H. Abe NH MI SY H. Aikata TK YK RA KC. Analyzed the data: CNH SA MT DM HO KC. Contributed reagents/materials/analysis tools: CNH SA MT DM KC. Wrote the paper: CNH SA MT DM KC. Clinical data: KC MT DM HAB NH MI ST HAI TK YK WO. Obtained funding: KC MT DM. Critical review of the manuscript: CNH SA MT DM RA HAB HO NH MI ST HAI TK YK WO KC.

## References

1. Fields BN, Knipe DM, Howley PM (2007) Fields virology. Philadelphia: Wolters Kluwer Health/Lippincott Williams & Wilkins.
2. McMahon BJ (2009) The natural history of chronic hepatitis B virus infection. Hepatology 49: S45–55.
3. Brechot C, Kremsdorf D, Soussan P, Pineau P, Dejean A, et al. (2010) Hepatitis B virus (HBV)-related hepatocellular carcinoma (HCC): molecular mechanisms and novel paradigms. Pathologie-biologie 58: 278–287.
4. Ji F, Yang B, Peng X, Ding H, You H, et al. (2011) Circulating microRNAs in hepatitis B virus-infected patients. Journal of viral hepatitis 18: e242–251.
5. Novellino L, Rossi RL, Bonino F, Cavallone D, Abrignani S, et al. (2012) Circulating Hepatitis B Surface Antigen Particles Carry Hepatocellular microRNAs. PloS one 7: e31952.
6. Qi P, Cheng SQ, Wang H, Li N, Chen YF, et al. (2011) Serum MicroRNAs as Biomarkers for Hepatocellular Carcinoma in Chinese Patients with Chronic Hepatitis B Virus Infection. PloS one 6: e28486.
7. Ura S, Honda M, Yamashita T, Ueda T, Takatori H, et al. (2009) Differential microRNA expression between hepatitis B and hepatitis C leading disease progression to hepatocellular carcinoma. Hepatology 49: 1098–1112.

8. Zhang GL, Li YX, Zheng SQ, Liu M, Li X, et al. (2010) Suppression of hepatitis B virus replication by microRNA-199a-3p and microRNA-210. Antiviral research 88: 169–175.
9. Chen Y, Cheng G, Mahato RI (2008) RNAi for treating hepatitis B viral infection. Pharmaceutical research 25: 72–86.
10. Xi Y, Nakajima G, Gavin E, Morris CG, Kudo K, et al. (2007) Systematic analysis of microRNA expression of RNA extracted from fresh frozen and formalin-fixed paraffin-embedded samples. RNA 13: 1668–1674.
11. Turchinovich A, Weiz L, Langheinz A, Burwinkel B (2011) Characterization of extracellular circulating microRNA. Nucleic acids research 39: 7223–7233.
12. Liu AM, Zhang C, Burchard J, Fan ST, Wong KF, et al. (2011) Global regulation on microRNA in hepatitis B virus-associated hepatocellular carcinoma. Omics : a journal of integrative biology 15: 187–191.
13. Bala S, Marcos M, Szabo G (2009) Emerging role of microRNAs in liver diseases. World journal of gastroenterology : WJG 15: 5633–5640.
14. Desmet VJ, Gerber M, Hoofnagle JH, Manns M, Scheuer PJ (1994) Classification of chronic hepatitis: diagnosis, grading and staging. Hepatology 19: 1513–1520.
15. Tsuge M, Hiraga N, Takaishi H, Noguchi C, Oga H, et al. (2005) Infection of human hepatocyte chimeric mouse with genetically engineered hepatitis B virus. Hepatology 42: 1046–1054.
16. Weibrecht I, Leuchowius KJ, Clausson CM, Conze T, Jarvius M, et al. (2010) Proximity ligation assays: a recent addition to the proteomics toolbox. Expert review of proteomics 7: 401–409.
17. Cullen BR (2011) Viruses and microRNAs: RISCy interactions with serious consequences. Genes & development 25: 1881–1894.
18. Wang Y, Kato N, Jazag A, Dharel N, Otsuka M, et al. (2006) Hepatitis C virus core protein is a potent inhibitor of RNA silencing-based antiviral response. Gastroenterology 130: 883–892.
19. Ren M, Qin D, Li K, Qu J, Wang L, et al. (2012) Correlation between hepatitis B virus protein and microRNA processor Drosha in cells expressing HBV. Antiviral research.
20. Wang S, Qiu L, Yan X, Jin W, Wang Y, et al. (2011) Loss of MiR-122 expression in patients with hepatitis B enhances hepatitis B virus replication through cyclin G1 modulated P53 activity. Hepatology 55: 730–741.
21. Hu J, Xu Y, Hao J, Wang S, Li C, et al. (2012) MiR-122 in hepatic function and liver diseases. Protein & cell 3: 364–371.
22. Chang J, Nicolas E, Marks D, Sander C, Lerro A, et al. (2004) miR-122, a mammalian liver-specific microRNA, is processed from hcr mRNA and may downregulate the high affinity cationic amino acid transporter CAT-1. RNA biology 1: 106–113.
23. Narbus CM, Israelow B, Sourisseau M, Michta ML, Hopcraft SE, et al. (2011) HepG2 cells expressing microRNA miR-122 support the entire hepatitis C virus life cycle. Journal of virology 85: 12087–12092.
24. Shimakami T, Yamane D, Jangra RK, Kempf BJ, Spaniel C, et al. (2012) Stabilization of hepatitis C virus RNA by an Ago2-miR-122 complex. Proceedings of the National Academy of Sciences of the United States of America 109: 941–946.
25. Wilson JA, Zhang C, Huys A, Richardson CD (2011) Human Ago2 is required for efficient microRNA 122 regulation of hepatitis C virus RNA accumulation and translation. Journal of virology 85: 2342–2350.
26. Wang S, Qiu L, Yan X, Jin W, Wang Y, et al. (2012) Loss of microRNA 122 expression in patients with hepatitis B enhances hepatitis B virus replication through cyclin G(1) -modulated P53 activity. Hepatology 55: 730–741.
27. Chen Y, Shen A, Rider PJ, Yu Y, Wu K, et al. (2011) A liver-specific microRNA binds to a highly conserved RNA sequence of hepatitis B virus and negatively regulates viral gene expression and replication. The FASEB journal : official publication of the Federation of American Societies for Experimental Biology 25: 4511–4521.
28. Qiu L, Fan H, Jin W, Zhao B, Wang Y, et al. (2010) miR-122-induced down-regulation of HO-1 negatively affects miR-122-mediated suppression of HBV. Biochemical and biophysical research communications 398: 771–777.
29. Waidmann O, Bihrer V, Pleli T, Farnik H, Berger A, et al. (2012) Serum microRNA-122 levels in different groups of patients with chronic hepatitis B virus infection. Journal of viral hepatitis 19: e58–65.
30. Heermann KH, Goldmann U, Schwartz W, Seyffarth T, Baumgarten H, et al. (1984) Large surface proteins of hepatitis B virus containing the pre-s sequence. Journal of virology 52: 396–402.
31. Patient R, Hourioux C, Sizaret PY, Trassard S, Sureau C, et al. (2007) Hepatitis B virus subviral envelope particle morphogenesis and intracellular trafficking. Journal of virology 81: 3842–3851.
32. Bouttier M, Saumet A, Peter M, Courgnaud V, Schmidt U, et al. (2012) Retroviral GAG proteins recruit AGO2 on viral RNAs without affecting RNA accumulation and translation. Nucleic acids research 40: 775–786.
33. Eulalio A, Behm-Ansmant I, Schweizer D, Izaurralde E (2007) P-body formation is a consequence, not the cause, of RNA-mediated gene silencing. Molecular and cellular biology 27: 3970–3981.
34. Lian SL, Li S, Abadal GX, Pauley BA, Fritzler MJ, et al. (2009) The C-terminal half of human Ago2 binds to multiple GW-rich regions of GW182 and requires GW182 to mediate silencing. RNA 15: 804–813.
35. Giner A, Lakatos L, Garcia-Chapa M, Lopez-Moya JJ, Burgyan J (2010) Viral protein inhibits RISC activity by argonaute binding through conserved WG/GW motifs. PLoS pathogens 6: e1000996.
36. Johnston M, Geoffroy MC, Sobala A, Hay R, Hutvagner G (2010) HSP90 protein stabilizes unloaded argonaute complexes and microscopic P-bodies in human cells. Molecular biology of the cell 21: 1462–1469.
37. Pare JM, Tahbaz N, Lopez-Orozco J, LaPointe P, Lasko P, et al. (2009) Hsp90 regulates the function of argonaute 2 and its recruitment to stress granules and P-bodies. Molecular biology of the cell 20: 3273–3284.
38. Lan YT, Li J, Liao W, Ou J (1999) Roles of the three major phosphorylation sites of hepatitis B virus core protein in viral replication. Virology 259: 342–348.
39. Rudel S, Wang Y, Lenobel R, Korner R, Hsiao HH, et al. (2011) Phosphorylation of human Argonaute proteins affects small RNA binding. Nucleic acids research 39: 2330–2343.
40. Zeng Y, Sankala H, Zhang X, Graves PR (2008) Phosphorylation of Argonaute 2 at serine-387 facilitates its localization to processing bodies. The Biochemical journal 413: 429–436.
41. Sir D, Tian Y, Chen WL, Ann DK, Yen TS, et al. (2010) The early autophagic pathway is activated by hepatitis B virus and required for viral DNA replication. Proceedings of the National Academy of Sciences of the United States of America 107: 4383–4388.
42. Li J, Liu Y, Wang Z, Liu K, Wang Y, et al. (2011) Subversion of cellular autophagy machinery by hepatitis B virus for viral envelopment. Journal of virology 85: 6319–6333.
43. Sir D, Ann DK, Ou JH (2010) Autophagy by hepatitis B virus and for hepatitis B virus. Autophagy 6.
44. Potenza N, Papa U, Mosca N, Zerbini F, Nobile V, et al. (2011) Human microRNA hsa-miR-125a-5p interferes with expression of hepatitis B virus surface antigen. Nucleic acids research 39: 5157–5163.
45. Zhang X, Zhang E, Ma Z, Pei R, Jiang M, et al. (2011) Modulation of hepatitis B virus replication and hepatocyte differentiation by MicroRNA-1. Hepatology 53: 1476–1485.
46. Hu W, Wang X, Ding X, Li Y, Zhang X, et al. (2012) MicroRNA-141 Represses HBV Replication by Targeting PPARA. PloS one 7: e34165.
47. Li D, Liu X, Lin L, Hou J, Li N, et al. (2011) MicroRNA-99a inhibits hepatocellular carcinoma growth and correlates with prognosis of patients with hepatocellular carcinoma. The Journal of biological chemistry 286: 36677–36685.
48. Turcatel G, Rubin N, El-Hashash A, Warburton D (2012) MIR-99a and MIR-99b modulate TGF-beta induced epithelial to mesenchymal plasticity in normal murine mammary gland cells. PloS one 7: e31032.
49. Murata M, Matsuzaki K, Yoshida K, Sekimoto G, Tahashi Y, et al. (2009) Hepatitis B virus X protein shifts human hepatic transforming growth factor (TGF)-beta signaling from tumor suppression to oncogenesis in early chronic hepatitis B. Hepatology 49: 1203–1217.
50. Xu D, Takeshita F, Hino Y, Fukunaga S, Kudo Y, et al. (2011) miR-22 represses cancer progression by inducing cellular senescence. The Journal of cell biology 193: 409–424.
51. Jiang R, Deng L, Zhao L, Li X, Zhang F, et al. (2011) miR-22 promotes HBV-related hepatocellular carcinoma development in males. Clinical cancer research: an official journal of the American Association for Cancer Research 17: 5593–5603.

nature genetics

# Whole-genome sequencing of liver cancers identifies etiological influences on mutation patterns and recurrent mutations in chromatin regulators

Akihiro Fujimoto[1,16], Yasushi Totoki[2,16], Tetsuo Abe[1], Keith A Boroevich[1], Fumie Hosoda[2], Ha Hai Nguyen[1], Masayuki Aoki[1], Naoya Hosono[1], Michiaki Kubo[1], Fuyuki Miya[1], Yasuhito Arai[2], Hiroyuki Takahashi[2], Takuya Shirakihara[2], Masao Nagasaki[3], Tetsuo Shibuya[3], Kaoru Nakano[1], Kumiko Watanabe-Makino[1], Hiroko Tanaka[3], Hiromi Nakamura[2], Jun Kusuda[4], Hidenori Ojima[5], Kazuaki Shimada[6], Takuji Okusaka[7], Masaki Ueno[8], Yoshinobu Shigekawa[8], Yoshiiku Kawakami[9], Koji Arihiro[10], Hideki Ohdan[11], Kunihito Gotoh[12], Osamu Ishikawa[12], Shun-ichi Ariizumi[13], Masakazu Yamamoto[13], Terumasa Yamada[12], Kazuaki Chayama[1,9], Tomoo Kosuge[6], Hiroki Yamaue[8], Naoyuki Kamatani[1], Satoru Miyano[3], Hitoshi Nakagama[5,14], Yusuke Nakamura[1,15], Tatsuhiko Tsunoda[1], Tatsuhiro Shibata[2] & Hidewaki Nakagawa[1]

**Hepatocellular carcinoma (HCC) is the third leading cause of cancer-related death worldwide. We sequenced and analyzed the whole genomes of 27 HCCs, 25 of which were associated with hepatitis B or C virus infections, including two sets of multicentric tumors. Although no common somatic mutations were identified in the multicentric tumor pairs, their whole-genome substitution patterns were similar, suggesting that these tumors developed from independent mutations, although their shared etiological backgrounds may have strongly influenced their somatic mutation patterns. Statistical and functional analyses yielded a list of recurrently mutated genes. Multiple chromatin regulators, including *ARID1A*, *ARID1B*, *ARID2*, *MLL* and *MLL3*, were mutated in ~50% of the tumors. Hepatitis B virus genome integration in the *TERT* locus was frequently observed in a high clonal proportion. Our whole-genome sequencing analysis of HCCs identified the influence of etiological background on somatic mutation patterns and subsequent carcinogenesis, as well as recurrent mutations in chromatin regulators in HCCs.**

To gain insight into the molecular alterations of virus-associated HCC, we performed whole-genome sequencing (WGS) of 27 HCC tumors from 25 affected individuals, including two sets of multicentric tumors (MCTs) and matched normal lymphocytes (**Supplementary Table 1**). This included 11 hepatitis B virus (HBV)-related HCCs, 14 hepatitis C virus (HCV)-related HCCs and 2 HCCs without HBV or HCV infection (NBNC). Two affected individuals (HC3 and HC7) had two independent synchronous tumors, which were determined to be MCTs, not intrahepatic metastases, on the basis of their clinicopathological features. After PCR duplication removal, we obtained an average of 39.8× (tumor) and 32.7× (lymphocyte) coverage of the genomes by uniquely mapping 50–125 bp reads using paired-end sequencing (**Supplementary Fig. 1**). We identified somatic point mutations and indels with a false positive rate of less than 5% and 10%, respectively (**Supplementary Note**). We detected 4,886–24,147 somatic point mutations per tumor (**Fig. 1a** and **Supplementary Table 2**), and the average number of somatic point mutations at the whole-genome level was 4.2 per megabase. One tumor (HC11), which exhibited an exceptionally large number of somatic mutations (24,147 substitutions with predominant C>T/G>A transition at CpGs and 8,950 indels; **Fig. 1a**), was determined to have a DNA mismatch-repair defect due to a somatic nonsense mutation (encoding p.Glu234*) in *MLH1*. Analysis of the ratio of the depth of coverage identified 294 deleted regions ($\log_2$R ratio $\leq -1$) and 20 amplified regions ($\log_2$R ratio $\geq 2$) (**Supplementary Table 3** and **Supplementary Note**). Inconsistencies in mapped reads and subsequent PCR validation identified an average

[1]Center for Genomic Medicine, RIKEN, Yokohama, Japan. [2]Division of Cancer Genomics, National Cancer Center Research Institute, Tokyo, Japan. [3]Laboratory of DNA Informatics Analysis, Human Genome Center, Institute of Medical Science, The University of Tokyo, Tokyo, Japan. [4]National Institute of Biomedical Innovation, Ibaraki, Osaka, Japan. [5]Division of Molecular Pathology, National Cancer Center Research Institute, Tokyo, Japan. [6]Hepatobiliary and Pancreatic Surgery Division, National Cancer Center Hospital, Tokyo, Japan. [7]Hepatobiliary and Pancreatic Oncology Division, National Cancer Center Hospital, Tokyo, Japan. [8]Department of Gastroenterological Surgery, Wakayama Medical University, Wakayama, Japan. [9]Department of Medicine & Molecular Science, Hiroshima University School of Medicine, Hiroshima, Japan. [10]Department of Gastroenterological Surgery, Hiroshima University School of Medicine, Hiroshima, Japan. [11]Department of Anatomical Pathology, Hiroshima University School of Medicine, Hiroshima, Japan. [12]Department of Surgery, Osaka Medical Center for Cancer and Cardiovascular Diseases, Osaka, Japan. [13]Department of Gastroenterological Surgery, Tokyo Women's Medical University, Tokyo, Japan. [14]Division of Cancer Development System, National Cancer Center Research Institute, Tokyo, Japan. [15]Laboratory of Molecular Medicine, Human Genome Center, Institute of Medical Science, The University of Tokyo, Tokyo, Japan. [16]These authors contributed equally to this work. Correspondence should be addressed to H. Nakagawa (hidewaki@ims.u-tokyo.ac.jp) or T. Shibata (tashibat@ncc.go.jp).

Received 17 January; accepted 30 April; published online 27 May 2012; doi:10.1038/ng.2291

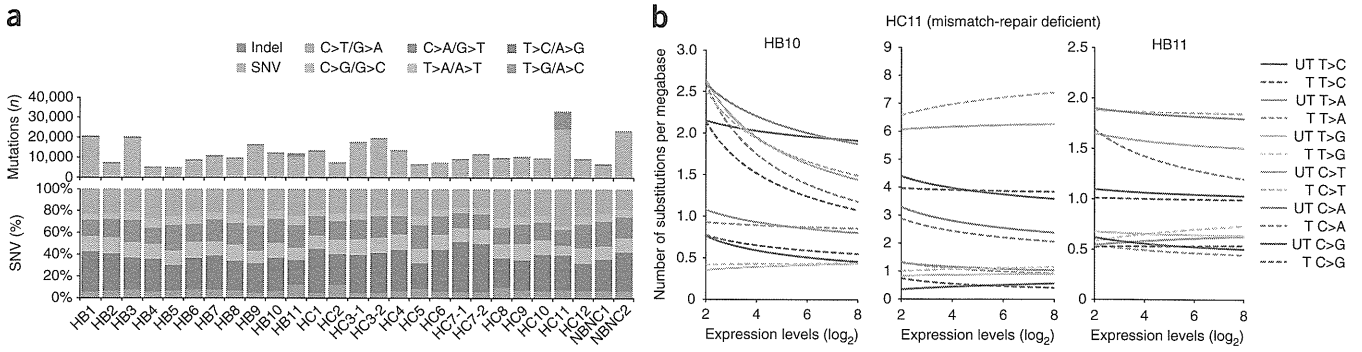


**Figure 1** Somatic substitution patterns of HCCs. (**a**) The number of somatic substitutions and indels (top) and somatic substitution patterns (bottom) of the 27 HCC genomes. (**b**) Repair on the transcribed strand. Fitted curves show the effect of gene expression and strand bias on substitution prevalence. We used Agilent microarray expression data (Whole Human Genome 8 × 60K Oligonucleotide Microarray) in this transcription-coupled repair (TCR) analysis, and expression level indicates Agilent microarray intensity level units with a $\log_2$ scale. UT, untranscribed strands; T, transcribed strands.

of 20.8 genomic rearrangements per tumor (**Supplementary Table 4** and **Supplementary Note**). The number of somatic substitutions, indels and rearrangements were not significantly different between HBV- and HCV-related HCCs (**Supplementary Fig. 2**).

The distribution of somatic substitutions in HCC genomes is significantly deviated from the assumption of a uniform mutation rate ($\chi$-square test; $P$ value $< 1 \times 10^{-300}$), and we identified a dominance of T>C/A>G transitions (odds ratio (OR) = 2.02, 95% confidence interval (CI) = 1.95–2.08; **Fig. 1a**), as described previously[1], as well as C>A/G>T transversions (OR = 1.43, 95% CI = 1.36–1.50) and C>T/G>A transitions (OR = 1.75, 95% CI = 1.68–1.82), particularly at CpG sites (OR = 4.55, 95% CI = 4.30–4.80) (**Supplementary Fig. 3**). As C>T/G>A transitions are also dominant in other cancers[2], T>C/A>G transitions and C>A/G>T transversions could be characteristic mutational signatures of HCC genomes.

To examine the influence of transcription-coupled repair, we compared gene expression levels (**Supplementary Tables 5** and **6**) and the number of substitutions in seven HCCs. Only T>C and C>A changes but not C>T changes were effectively repaired on the transcribed strand (**Supplementary Fig. 4a–c**), and these repairs occurred more frequently in highly expressing genes (HB10 in **Fig. 1b** and **Supplementary Fig. 5**). Of note, transcription-coupled repair did not occur in the mismatch repair–deficient tumor with *MLH1* inactivation (HC11 in **Fig. 1b**). Another case (HB11) had a familial disposition to cancer (**Supplementary Table 1**) and exhibited a distinct mutation signature (increased indels, less dominance of T>C/A>G transitions and a decreased effect of transcription-coupled repair at T>C transitions) (**Fig. 1a,b**), although no causal mutation explaining the DNA-repair deficiency was identified. These findings suggest that transcription-coupled repair preferentially repairs somatic substitutions that are specifically increased in cancer.

One of the characteristic features of HCC is multiple occurrences or MCTs in a strong carcinogenetic background. First, we compared somatic mutation sites of the two pairs of MCTs (HC3 and HC7). In protein-coding regions, no common somatic mutations were identified. *ATM*, *FSIP2* and *LRFN5* were mutated in both MCTs of HC3, but the locations of the mutations were different. In non-coding regions, WGS identified 30 and 37 common somatic point mutations and indels in the HC3 and HC7 pairs, respectively. However, most of these occurred in repetitive regions, and all candidates that could be analyzed by Sanger sequencing ($n$ = 20) were found to be germline variants (**Supplementary Note**). We also found no common structural alterations in these MCTs (**Fig. 2a**). These findings suggest that these synchronous MCTs developed through an accumulation of a completely different set of genetic alterations. Second, we applied

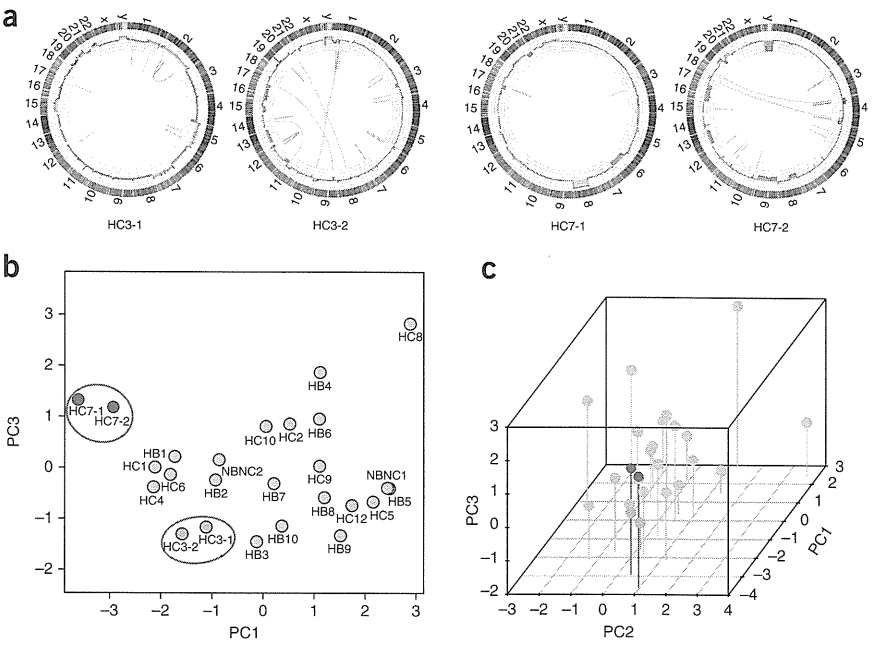


**Figure 2** Mutation patterns of MCTs. (**a**) Circos plots[20] of the MCTs from two subjects (HC3 and HC7). Each circle plot represents validated rearrangements (inner arcs) and copy-number alternations (inner rings). In rearrangements, lines show translocations (green), deletions (blue), inversions (orange) and tandem duplications (red). Copy-number gain and loss regions are shown in green and red. (**b**) PCA of the somatic substitution patterns of 25 HCC genomes. Two sets of MCT pairs (HC3 and HC7) are shown by green and blue, respectively, and are circled in red. (**c**) Three-dimensional plot of principal components (PCs) for 25 HCCs on somatic substitution pattern. Two sets of MCT pairs (HC3 and HC7) are shown in green and blue, respectively.

**Table 1 Significantly mutated genes and their mutation frequency in the validation set**

| Gene | Chr. | Start | End | CDS length (bp) | Coding indel | Missense | Nonsense | Splice site | Total | *P* value | *q* value | Frequency in validation set |
|---|---|---|---|---|---|---|---|---|---|---|---|---|
| *TP53* | 17 | 7,572,927 | 7,579,912 | 1,218 | 0 | 11 | 0 | 3 | 14 | 0 | 0 | NA |
| *ERRFI1* | 1 | 8,073,270 | 8,075,679 | 1,397 | 1 | 0 | 2 | 0 | 3 | 0.00020 | 0.0034 | 3.1% (2/65) |
| *ZIC3* | X | 136,648,851 | 136,652,229 | 1,412 | 0 | 3 | 0 | 0 | 3 | 0.00050 | 0.0041 | 3.3% (4/120) |
| *CTNNB1* | 3 | 41,265,560 | 41,280,833 | 2,398 | 0 | 3 | 0 | 0 | 3 | 0.0015 | 0.0071 | NA |
| *GXYLT1* | 12 | 42,481,588 | 42,538,448 | 1,351 | 0 | 3 | 0 | 0 | 3 | 0.0013 | 0.0071 | 0.8% (1/120) |
| *OTOP1* | 4 | 4,190,530 | 4,228,591 | 1,859 | 1 | 2 | 0 | 0 | 3 | 0.0015 | 0.0071 | 0.8% (1/120) |
| *ALB* | 4 | 74,270,045 | 74,286,015 | 1,882 | 3 | 0 | 0 | 0 | 3 | 0.0022 | 0.0089 | 3.3% (4/120) |
| *ATM* | 11 | 108,098,352 | 108,236,235 | 9,415 | 1 | 4 | 0 | 0 | 5 | 0.0037 | 0.013 | 5.0% (6/120) |
| *ZNF226* | 19 | 44,674,234 | 44,681,827 | 2,424 | 1 | 1 | 1 | 0 | 3 | 0.0043 | 0.014 | 3.3% (4/120) |
| *USP25* | 21 | 17,102,713 | 17,250,794 | 3,260 | 1 | 2 | 0 | 0 | 3 | 0.0051 | 0.015 | 0% (0/120) |
| *WWP1* | 8 | 87,386,280 | 87,479,122 | 2,857 | 2 | 1 | 0 | 0 | 3 | 0.0060 | 0.016 | 7.7% (5/65) |
| *IGSF10* | 3 | 151,154,477 | 151,176,497 | 7,892 | 0 | 4 | 0 | 0 | 4 | 0.0091 | 0.023 | 3.3% (4/120) |
| *ARID1A* | 1 | 27,022,895 | 27,107,247 | 6,934 | 2 | 1 | 0 | 0 | 3 | 0.011 | 0.026 | 10% (12/120) |
| *UBR3* | 2 | 170,684,018 | 170,938,353 | 5,819 | 0 | 3 | 0 | 0 | 3 | 0.018 | 0.041 | 0.8% (1/120) |
| *BAZ2B* | 2 | 160,176,776 | 160,335,230 | 6,643 | 0 | 3 | 0 | 0 | 3 | 0.024 | 0.050 | 1.6% (2/120) |

Significantly mutated genes with more than two mutations are shown. Chr., chromosome.

principal-component analysis (PCA) to further examine genome-wide somatic mutation patterns. Two HCCs (HC11 and HB11) exhibited quite distinct substitution patterns compared to the other samples due to their mismatch-repair deficiency (**Supplementary Fig. 6a**). Therefore, they were excluded from PCA. Notably, the pairs of each MCT (HC3 and HC7) were tightly clustered in PCA (permutation test; *P* value = 0.00050), indicating similar somatic substitution patterns on the whole-genome level (**Fig. 2b,c**). Considering that these MCTs shared the exact same genetic and environmental backgrounds, the somatic substitution patterns are likely to be determined by the etiological backgrounds in which the tumors developed.

We also examined associations between the principal components and clinical factors. Although the correlations between somatic substitution patterns and age at diagnosis, tumor grade, liver fibrosis and tumor size were not significant, habitual alcohol drinking and the occurrence of synchronous or metachronous multiple liver nodules showed significant association with principal components of the somatic substitution patterns (habitual alcohol drinking, $P = 0.028$; multiple liver nodules, $P = 0.016$) (**Supplementary Fig. 6b,c**). Virus type showed a marginal association with substitution pattern ($P = 0.091$) (**Supplementary Fig. 6d**). In addition to viral infection, alcohol abuse, obesity, diabetes and other metabolic disorders are also risk factors for liver carcinogenesis, and its background etiology is very heterogeneous[3]. Multiple background factors, including germline variants, epigenetic status of liver, virus infection, exposure to other environmental carcinogens, inflammation and a combination of these factors, would contribute to the somatic mutation pattern in cancer genomes.

Across all 27 HCC genomes, we detected a total of 2,048 (75.9 per tumor) protein-altering point mutations, including 1,734 missense mutations, 101 nonsense mutations, 161 short coding indels and 52 splice-site mutations (**Supplementary Table 2**). After adjusting for the regional deviation of somatic mutation rate and gene length, significantly frequent mutations were found to occur in 15 genes, with a false discovery rate (FDR) of ≤0.05 (**Table 1** and **Supplementary Table 7**). *TP53* and *CTNNB1* (encoding β-catenin) genes were significantly mutated in HCC, as previously reported[4]. Five mutations of *ATM* were detected in four tumors without *TP53* mutations. Sequencing analysis on an independent set of 120 HCCs detected 6 additional *ATM* mutations (5%) (**Table 1** and **Supplementary Table 8**). Three mutations of *ARID1A*, two frameshifts and one missense, were detected in three tumors by WGS. *ARID1A* encodes a key component of the SWI-SNF chromatin-remodeling complex, and *ARID1A* mutations have been detected in ovarian cancer[5] and many other cancers[6]. Sequencing analysis of the 120 HCCs detected 12 additional mutations of *ARID1A* (10%) (**Table 1** and **Supplementary Table 8**). WGS detected three somatic mutations in *ERRFI1*, two nonsense and one frameshift, in two tumors. *ERRFI1* encodes a protein that inhibits the kinase domains of EGFR and ERBB2 (ref. 7), and *Errfi1* knockout mice showed enhanced hepatocyte proliferation[8]. These mutations may cause the loss of inhibitory function and thereby activate the EGFR signaling pathway in HCC. We detected 2 additional mutations of *ERRFI1* (3.1%) in 65 independent HCCs (**Table 1** and **Supplementary Table 8**). Three

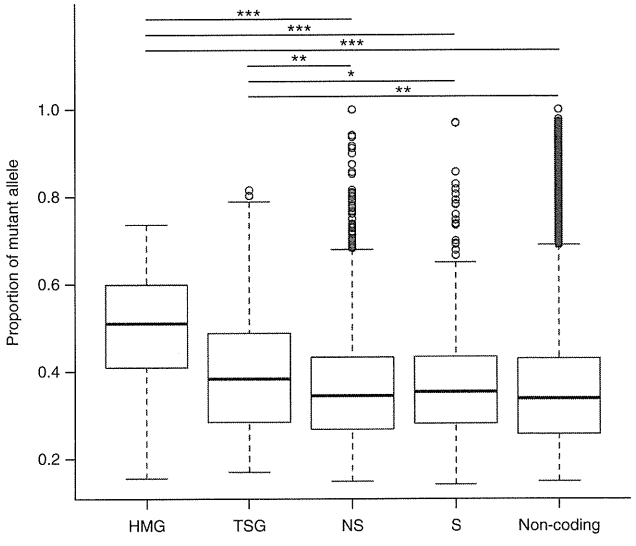


**Figure 3** Mutant allele proportions of point mutations. HMG, highly mutated genes, genes whose mutation frequency was greater than 3% in the validation set (*ARID1A, IGSF10, ATM, ZNF226, ZIC3, WWP1* and *ERRFI1*); TSG, known tumor suppressor genes annotated by MutationAssessor[21]; NS, nonsynonymous; S, synonymous. Non-coding includes point mutations in non-coding regions except for in splice sites. The edges of the boxes represent the 25th and 75th percentile values. The whiskers represent the most extreme data points, which are no more than 1.5 times the interquartile range from the boxes. $*P < 0.05$; $**P < 0.01$; $***P < 0.001$.

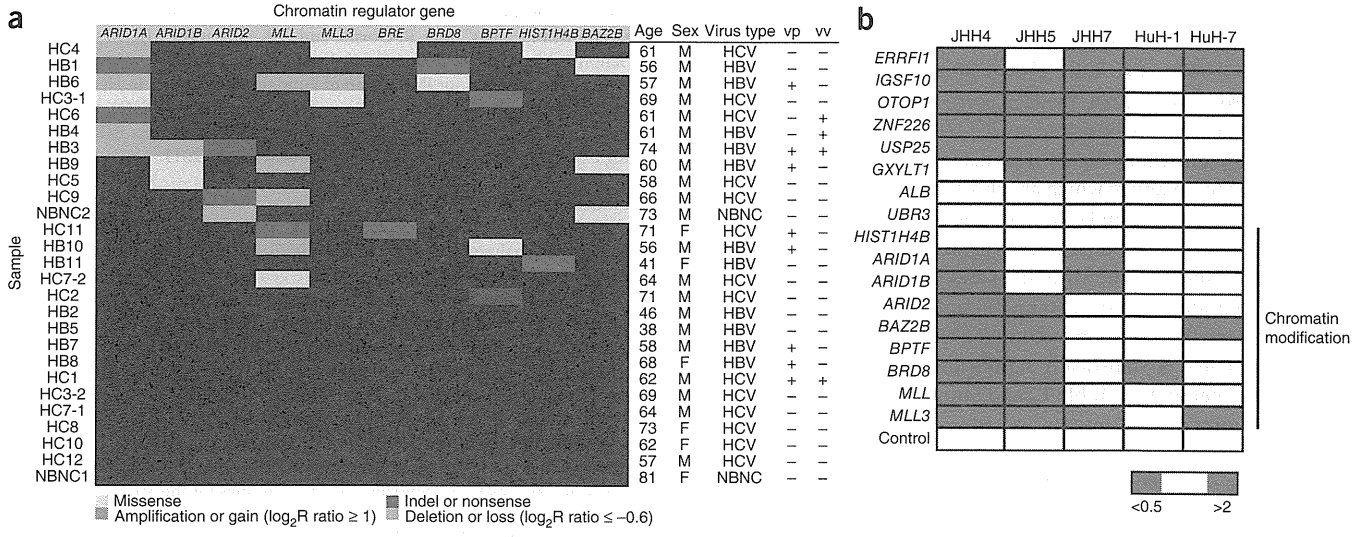


**Figure 4** Mutations in chromatin regulators and functional analysis of potential driver genes. (**a**) Mutations in chromatin regulators in 27 HCC genomes. Mutations in chromatin-regulator genes are summarized. In addition to point mutations, 55.6-kb genomic deletion of *ARID2* in NBNC2, which was identified by the read-pair method, and several copy-number alternations of chromatin-regulator genes are included. HC6 had both 1-bp deletion and low-level loss in *ARID1A*. (**b**) Functional assays of potential driver genes in HCC cell lines. Changes in cell proliferation in five HCCs compared to proliferation with control siRNA treatment are presented. Magenta and blue boxes represent more than 2-fold and less than 0.5-fold changes in the cell number, respectively. Genes involved in chromatin modification are indicated by the line.

mutations of *WWP1* were detected by WGS. *WWP1* encodes an E3 ubiquitin ligase that affects protein stability of some oncogenes, such as ERBB4 (ref. 9). We also detected 5 additional mutations (7.7%) of *WWP1* in 65 HCCs (**Table 1** and **Supplementary Table 8**). We detected additional mutations of *IGSF10*, *ZNF226*, *ZIC3* and *ALB*, each at a 3% frequency (**Table 1** and **Supplementary Table 8**), but their functional significance in cancer is unknown. Next, we compared the mutant allele proportions of point mutations in highly mutated genes whose frequency was validated (*ARID1A*, *IGSF10*, *ATM*, *ZNF226*, *ZIC3*, *WWP1* and *ERRFI1*) among the significantly mutated genes, known tumor suppressor genes and non-coding regions. The proportions of point mutation alleles of both highly mutated genes and tumor suppressor genes were significantly higher than that of non-coding regions (**Fig. 3**), which indicates that either the wild-type alleles were deleted or mutations in these genes were generated in the ancestral cell population of tumor cells. The mutant allele proportion or mutation clonality within a tumor would provide useful information to identify driver mutations[10].

To identify biologically relevant mutations in HCCs, we performed gene-set enrichment (GSE) analysis on the mutated genes[11].

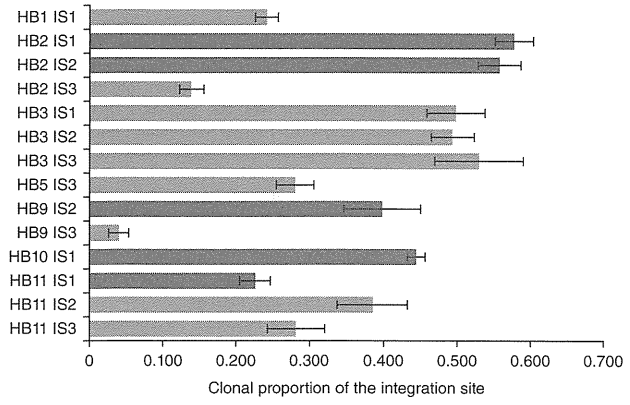


We attempted to enrich functional mutations by selecting genes with deleterious mutations (nonsense, indel and splice-site mutations). In GSE analysis, the 'bromodomain' and 'chromatin-regulator' gene sets were found to be significantly enriched in the mutated gene list (**Supplementary Table 9**). WGS detected recurrent somatic mutations in several genes annotated to be associated with chromatin regulation, such as *ARID1A*, *ARID1B*, *ARID2*, *MLL*, *MLL3*, *BAZ2B*, *BRD8*, *BPTF*, *BRE* and *HIST1H4B*. Notably, 14 out of the 27 tumors (52%) had somatic point mutations or indels in at least one of these chromatin regulators (**Fig. 4a** and **Supplementary Tables 7** and **10**). Sequencing analysis of the 120 independent HCCs detected 8 additional mutations of *ARID1B* (6.7%), 7 of *ARID2* (5.8%), 5 of *MLL3* (4.2%), 2 of *MLL* (1.7%) and 2 of *BPTF* (1.7%), as well as 12 of *ARID1A* (10%) (**Supplementary Tables 8** and **10**). In both the WGS and the validation set, the number of indels was significantly higher in chromatin regulators than in genes in other categories ($P = 2.1 \times 10^{-10}$; indel/nonsynonymous: 23/38 in chromatin regulators and 154/1,820 in genes in other categories), suggesting that loss-of-function mutations are enriched in these chromatin-regulator genes in HCC genomes. We observed that mutations in chromatin regulators were marginally associated with the stage of liver fibrosis and hepatic vein invasion (**Fig. 4a** and **Supplementary Table 11**), supporting the idea that mutations of chromatin regulators or the *ARID* family may contribute to poor prognosis for individuals with HCC.

To determine whether the recurrently mutated genes have any biological affect in HCC, we knocked down 17 candidate driver genes, including the chromatin regulators, through small interfering RNA (siRNA) in a panel of five HCC cell lines (**Supplementary Fig. 7**). Downregulation

**Figure 5** Clonal proportion of HBV integration sites in cancer cell populations of four HBV-integrated HCCs. Integration sites (ISs) in the *TERT* locus are indicated by red. Digital PCR analysis indicates 4.0–57.8% clonal population of HBV integration at each locus. The average proportion of the *TERT* integration sites (41%) was higher than that of other integration sites (32%). Error bars, s.e.m. from four replicate measures.

of three genes (*ERRFI1*, *IGSF10* and *MLL3*) promoted cell proliferation in four out of five HCC cell lines when compared to those treated with control siRNA (**Fig. 4b**). Knockdown of another eleven genes promoted cell growth in at least one HCC cell line (**Fig. 4b**). The growth-promoting effect was not observed in HCC cell lines that did not express the gene (**Supplementary Fig. 8**). This data implicates that these candidate driver genes, many of which are chromatin regulators, may have a tumor suppressive effect in HCC cells. The mutated chromatin regulators in HCC may change their target's gene expression though diverse remodeling of nucleosome structures and histone modification[12–14]. Moreover, multiple long non-coding RNAs, suggested to regulate chromatin status and transcription by coupling with chromatin regulators[15], were also mutated at statistically significant frequencies in our WGS analysis (**Supplementary Table 12** and **Supplementary Note**).

We determined HBV integration sites using sequence read-pair mapping information[16]. Twenty-three breakpoints were predicted by 3 or more supporting read-pairs and all were validated by PCR and Sanger sequencing. The breakpoints within the HBV genome were primarily localized to the downstream region of the *HBx* gene whereby deletion of C-terminal region may contribute to development of HCC (**Supplementary Fig. 9**). Interestingly, HBV genome integration was observed within or upstream of the *TERT* gene in four HBV-related HCCs as previously observed[17] (**Supplementary Fig. 10** and **Supplementary Table 13**). Using digital PCR, we quantified the clonal population with HBV integration in seven HBV-integrated HCCs and corresponding non-cancerous liver tissues, and the proportion of the integrated alleles ranged from 4.0% to 57.8% in the tumors (**Fig. 5**), while no clonal integration breakpoint was detected in the paired non-cancerous liver tissues. Considering HBV genome integration is an early event during chronic HBV infection[18], HBV integration in the *TERT* locus may confer clonal advantage in the early phase of HBV-related liver carcinogenesis.

This study provides a comprehensive analysis of the mutational landscape of heterogeneous virus-associated HCC genomes. The variation in somatic substitution patterns in individual tumors may reflect different exposure to carcinogens, DNA repair defects and cellular origin[19]. Considering the high complexity and heterogeneity of HCCs of both etiological and genetic aspects, further molecular classification is required for appropriate diagnosis and therapy in personalized medicine.

**URLs.** Human Genome Center, The University of Tokyo, http://sc.hgc.jp/shirokane.html; ICGC, http://www.icgc.org/; Gene Expression Omnibus (GEO) database, http://www.ncbi.nlm.nih.gov/geo/; ICGC data portal, http://dcc.icgc.org/; human reference genome (GRCh37), http://www.ncbi.nlm.nih.gov/projects/genome/assembly/grc/human/.

## METHODS

Methods and any associated references are available in the online version of the paper.

**Accession codes.** Information on all point mutations and indels was deposited to the ICGC web site, and the data can be acquired from the ICGC Data Portal site. Microarray expression data are deposited at the Gene Expression Omnibus (GEO) database under the accession number GSE36390.

*Note: Supplementary information is available in the online version of the paper.*

ACKNOWLEDGMENTS

The supercomputing resource SHIROKANE was provided by the Human Genome Center at The University of Tokyo. The authors thank T. Urushidate, S. Ohashi, N. Okada, A. Kokubu and H. Shimizu at the National Cancer Center Research Institute and C. Inai, R. Ooishi, and R. Kitada at the RIKEN Center for Genomic Medicine for their technical assistances. This work was supported partially by the Program for Promotion of Fundamental Studies in Health Sciences of the National Institute of Biomedical Innovation (NIBIO), the National Cancer Center Research and Development Fund (23-A-8) and the RIKEN Strategic Research Program for R&D of President's Fund 2011.

AUTHOR CONTRIBUTIONS

A.F., Y.T., T.A., K.A.B., F.M., H. Nakamura, T.T., T. Shibata and H. Nakagawa performed data analyses. F.H., Y.A., H. Takahashi, T. Shirakihara, K.N., K.W.-M., T. Shibata and H. Nakagawa performed whole-genome sequencing. F.H., H.H.N., K.N. and K.W.-M. performed the validation sequencing study. F.H., Y.A., H. Takahashi, T. Shirakihara and T. Shibata performed siRNA experiments. A.F., M.A., N.H. and M.K. performed digital PCR and SNP microarray experiments. M.N., T. Shibuya, H. Tanaka and S.M. operated the supercomputer system. H. Ojima, K.S., T.O., M.U., Y.S., Y.K., K.A., H. Ohdan, K.G., O.I., S.A., M.Y., T.Y., K.C., T.K. and H.Y. collected clinical samples. A.F., Y.T., T.T., T. Shibata and H. Nakagawa wrote the manuscript. Y.N., T.T., T. Shibata and H. Nakagawa conceived the study and led the design of the experiments. J.K., N.K., H. Nakagama, Y.N., T. Shibata and H. Nakagawa contributed to the findings for this study.

COMPETING FINANCIAL INTERESTS

The authors declare no competing financial interests.

Published online at http://www.nature.com/doifinder/10.1038/ng.2291.
Reprints and permissions information is available online at http://www.nature.com/reprints/index.html.

1. Totoki, Y. *et al.* High-resolution characterization of a hepatocellular carcinoma genome. *Nat. Genet.* **43**, 464–469 (2011).
2. Greenman, C. *et al.* Patterns of somatic mutation in human cancer genomes. *Nature* **446**, 153–158 (2007).
3. El-Serag, H.B. & Rudolph, K.L. Hepatocellular carcinoma: epidemiology and molecular carcinogenesis. *Gastroenterology* **132**, 2557–2576 (2007).
4. Laurent-Puig, P. & Zucman-Rossi, J. Genetics of hepatocellular tumors. *Oncogene* **25**, 3778–3786 (2006).
5. Wiegand, K.C. *et al. ARID1A* mutations in endometriosis-associated ovarian carcinomas. *N. Engl. J. Med.* **363**, 1532–1543 (2010).
6. Jones, S. *et al.* Somatic mutations in the chromatin remodeling gene *ARID1A* occur in several tumor types. *Hum. Mutat.* **33**, 100–103 (2012).
7. Ferby, I. *et al.* Mig6 is a negative regulator of EGF receptor–mediated skin morphogenesis and tumor formation. *Nat. Med.* **12**, 568–573 (2006).
8. Reschke, M. *et al.* Mitogen-inducible gene-6 is a negative regulator of epidermal growth factor receptor signaling in hepatocytes and human hepatocellular carcinoma. *Hepatology* **51**, 1383–1390 (2010).
9. Li, Y., Zhou, Z., Alimandi, M. & Chen, C. WW domain containing E3 ubiquitin protein ligase 1 targets the full-length ErbB4 for ubiquitin-mediated degradation in breast cancer. *Oncogene* **28**, 2948–2958 (2009).
10. Shah, S.P. *et al.* The clonal and mutational evolution spectrum of primary triple-negative breast cancers. *Nature* published online doi:10.1038/nature10933 (4 April 2012).
11. Huang, W., Sherman, B.T. & Lempicki, R.A. Bioinformatics enrichment tools: paths toward the comprehensive functional analysis of large gene lists. *Nucleic Acids Res.* **37**, 1–13 (2009).
12. Parsons, D.W. *et al.* The genetic landscape of the childhood cancer medulloblastoma. *Science* **331**, 435–439 (2011).
13. Varela, I. *et al.* Exome sequencing identifies frequent mutation of the SWI/SNF complex gene *PBRM1* in renal carcinoma. *Nature* **469**, 539–542 (2011).
14. Lee, J. *et al.* A tumor suppressive coactivator complex of p53 containing ASC-2 and histone H3-lysine-4 methyltransferase MLL3 or its paralogue MLL4. *Proc. Natl. Acad. Sci. USA* **106**, 8513–8518 (2009).
15. Khalil, A.M. *et al.* Many human large intergenic noncoding RNAs associate with chromatin-modifying complexes and affect gene expression. *Proc. Natl. Acad. Sci. USA* **106**, 11667–11672 (2009).
16. Jiang, Z. *et al.* The effects of hepatitis B virus integration into the genomes of hepatocellular carcinoma patients. *Genome Res.* **22**, 593–601 (2012).
17. Paterlini-Bréchot, P. *et al.* Hepatitis B virus–related insertional mutagenesis occurs frequently in human liver cancers and recurrently targets human telomerase gene. *Oncogene* **22**, 3911–3916 (2003).
18. Shafritz, D.A., Shouval, D., Sherman, H.I., Hadziyannis, S.J. & Kew, M.C. Integration of hepatitis B virus DNA into the genome of liver cells in chronic liver disease and hepatocellular carcinoma. Studies in percutaneous liver biopsies and post-mortem tissue specimens. *N. Engl. J. Med.* **305**, 1067–1073 (1981).
19. Pleasance, E.D. *et al.* A comprehensive catalogue of somatic mutations from a human cancer genome. *Nature* **463**, 191–196 (2010).
20. Krzywinski, M. *et al.* Circos: an information aesthetic for comparative genomics. *Genome Res.* **19**, 1639–1645 (2009).
21. Reva, B., Antipin, Y. & Sander, C. Determinants of protein function revealed by combinatorial entropy optimization. *Genome Biol.* **8**, R232 (2007).

## ONLINE METHODS

**Clinical samples.** The clinical and pathological features of 25 subjects and their 27 HCCs that were used for WGS are shown (**Supplementary Table 1**). HBV-related tumors were defined by the presence of HB surface antigen (HBsAg) in serum, and HCV-related tumors were defined by the presence of antibody to HCV (HCVAb) in serum. NBNC tumor was defined by a lack of both HBsAg and HCVAb. All subjects had undergone partial hepatectomy, and pathologists confirmed HCC with more than 80% viable tumor cells. High molecular weight genomic DNA was extracted from fresh-frozen tumor specimens and blood. All subjects agreed with informed consent to participate in the study following ICGC guidelines[22]. Ethical committees at RIKEN, the National Cancer Center and all groups participating in this study approved this work.

**Whole-genome sequencing.** We prepared insert libraries of 300–500 bp from 1.5–3 μg of genomic DNA from tumors and lymphocytes and sequenced them using the Illumina Genome Analyzer II and HiSeq 2000 platforms with paired-end reads of 50–125 bp according to the manufacturer's instructions.

**Somatic point mutation and short indel calls.** Read sequences were mapped by Burrows-Wheeler Aligner (BWA)[23] to the human reference genome (GRCh37). Possible PCR duplicate reads were removed by SAMtools[24] and in-house software. After filtering by pair mapping distance, mapping uniqueness and orientation between paired reads, the mapping result files were converted into the pileup format with SAMtools. Mutation calling was conducted in part on the basis of methods we have published elsewhere[1,25]. A detailed explanation is provided in the **Supplementary Note.**

**Identification of significantly mutated genes.** Because the number of mutations in a gene is influenced by gene length and the background mutation rate, we calculated the probability of the number of protein-altering mutations under the given mutation rate and gene length using the following set of calculations. First, we divided the genomic region into 1-Mb bins and estimated the mutation rates for point mutations and indels. Because the mutation rates in CpG sites were much higher than those of other regions (**Supplementary Fig. 3**), we estimated the mutation rate for point mutations in CpG and non-CpG sites separately. We used mutations in non-coding regions for mutation rate estimation. Second, the number of nonsynonymous sites was counted for each gene. Finally, the expected number of mutations in each gene was calculated by the total number of nonsynonymous sites and the background mutation rate. Tests of significance for each gene were performed by assuming a Poisson distribution. We adjusted for multiple testing using the Benjamini-Hochberg method[26].

**Somatic genomic rearrangement calls.** To identify genomic rearrangements, we used inconsistent and stretched read pairs that were uniquely mapped. We discarded read pairs with mapping quality of <30 and those with proper orientation and a distance between read pairs of <1 kb. If candidate rearrangements were supported by three or more read pairs and no rearrangement breakpoint was called within 500 bp of the tumor breakpoint in the matched lymphocyte sample, then we performed realignment to GRCh37 with blastn[27], and candidates supported by uniquely mapped read pairs were used for the validation study. We also discarded candidates that were not supported by at least one perfect-match read pair. We performed PCR validation of the candidates. Although only 10% of candidates that were supported by three read-pairs were validated, 74.1% of candidates supported by ≥4 read pairs were successfully validated (**Supplementary Fig. 11**).

**Somatic copy-number alteration calling.** We estimated copy-number alteration (CNA) over 5-kb windows. The ratio of standardized average depth between lymphocyte and cancer samples ($\log_2$R ratio) was calculated. CNA regions were defined by DNAcopy[28]. Segments with a $\log_2$R ratio of ≥2 or ≤−1 in two or more samples were considered as recurrent amplifications or deletions, respectively. Segments with a $\log_2$R ratio of ≥1 or ≤−0.6 in five or more samples were considered as recurrent gain (low-level amplification) and loss (low-level loss) regions, respectively.

**HBV integration calls.** To find HBV genome sequences in the tumor genome, we mapped read sequences to the genome of HBV genotype C (GenBank Nucleotide, NC_003977.1), which is most prevalent in Japan and east Asia. Our WGS analysis detected HBV genomic sequence in 8 out of 11 genomes of HBV-related HCCs. This is consistent with the previous observation that the HBV genomic sequence was not detected in cancerous or non-cancerous liver tissue in 20–35% of individuals with HCC that had HBsAg-positive sera[29,30]. To identify HBV integration sites, we selected read pairs in which one read was mapped to the HBV genome and the other was mapped to the human reference genome GRCh37. Twenty-three candidate sites were supported by three or more read pairs. We performed PCR validation of these candidates, and all candidates supported by three or more read pairs were successfully validated, and the breakpoints identified by Sanger sequencing were near the breakpoints predicted by the paired-end method.

**PCA of the somatic substitution pattern.** By comparing the genomes between the tumor and control sample from each affected subject, we counted the number of somatic mutations stratifying with substitution patterns, including C>A/G>T, C>G/G>C and C>T/G>A transversions at non-CpG sites, C>A/G>T, C>G/G>C and C>T/G>A transversions at CpG sites and T>A/A>T, T>C/A>G and T>G/A>C transversions. By dividing by the total substitution number within each individual $i$ with HCC, we calculated substitution frequencies for these nine groups as $f_{i1}, f_{i2}, \ldots f_{i9}$, respectively. Because they are normalized so that the sum of the frequencies from all groups = 1, we used vectors of the frequencies ($\mathbf{f}_{i1}, \mathbf{f}_{i2}, \ldots \mathbf{f}_{i9}$) ($i$ = 1–27) for PCA. PCA was implemented using the R command prcomp with the scaling option on. We used principal components that had eigenvalues of >1.0. For calculating correlation coefficients between the principal-component score vectors and phenotypes of HCC (for example, HBV/HCV/NBNC classification), we used a canonical correlation analysis and tested Wilks' $\lambda$ values to evaluate significance. Two HCCs (HC11 and HB11) showed quite distinct substitution patterns compared to others due to deficiency in DNA mismatch repair (**Supplementary Fig. 6a**) and were therefore excluded from PCA. PCA for other mutation sets was also performed (**Supplementary Table 14**). Also, we calculated correlation between each principal-component score and phenotypes across tumors. Similarities between the MCTs were examined by permutation test (**Supplementary Note**).

**Mutation validation by exon sequencing.** To discover recurrent mutations in HCCs, we amplified all protein-coding exons of the candidate genes using the DNA from 120 independent HCCs and their corresponding lymphocytes or non-cancerous livers and prepared the sequencing libraries from the amplicon mixture of pooled tumor DNA and pooled normal DNA. In total, we mixed 457 amplicons, corresponding to approximately 203 kb of DNA. The amplicon libraries were sequenced by HiSeq 2000. The average read depth per base was 174,141× and 198,103× for the tumor and non-tumor pools, respectively. We mixed in plasmid DNA as a negative control, and threshold frequencies were determined by the distribution of errors in plasmid DNA. Detailed methods have been described previously[31]. For some genes, we amplified each exon from DNA from a set of 65 HCCs and corresponding DNA from blood, and performed Sanger sequencing for each amplicon.

**Digital PCR.** The proportions of integration sites in cancer cell populations were examined using digital PCR[1,32]. We designed PCR primers to amplify integration sites and non-integration sites (**Supplementary Table 13**). Sequences for primers and probes are available upon request. The estimated frequencies of both integration sites (HB2-IS1 and HB2-IS2) were consistent, indicating that our estimation was highly reliable.

**siRNA transfection and measurement of cell proliferation.** Five HCC cell lines (JHH4, JHH5, JHH7, HuH-1 and HuH-7) were obtained from the Japanese Collection of Research Bioresources Cell Bank. Mixtures of three siRNAs targeting each gene and control, non-silencing siRNA were purchased (Thermo Fisher Scientific). Cell lines (1,000 cells) were seeded on 96-well plates and transfected with siRNA using Lipofectamine RNAiMAX (Invitrogen), according to the manufacturer's protocol. The number of cells in triplicate wells was measured by CellTiter96 AQueous One Solution Cell Proliferation Assay (Promega) on the sixth day after transfection.

22. Hudson, T.J. *et al.* International network of cancer genome projects. *Nature* **464**, 993–998 (2010).

23. Li, H. & Durbin, R. Fast and accurate short read alignment with Burrows-Wheeler transform. *Bioinformatics* **25**, 1754–1760 (2009).
24. Li, H. *et al.* The Sequence Alignment/Map format and SAMtools. *Bioinformatics* **25**, 2078–2079 (2009).
25. Fujimoto, A. *et al.* Whole-genome sequencing and comprehensive variant analysis of a Japanese individual using massively parallel sequencing. *Nat. Genet.* **42**, 931–936 (2010).
26. Benjamini, Y. & Hochberg, Y. Controlling the false discovery rate: a practical and powerful approach to multiple testing. *J. R. Stat. Soc. B* **57**, 289–300 (1995).
27. Altschul, S.F., Gish, W., Miller, W., Myers, E.W. & Lipman, D.J. Basic local alignment search tool. *J. Mol. Biol.* **215**, 403–410 (1990).
28. Andersson, R. *et al.* A segmental maximum a posteriori approach to genome-wide copy number profiling. *Bioinformatics* **24**, 751–758 (2008).
29. Zhou, Y.Z., Butel, J.S., Li, P.J., Finegold, M.J. & Melnick, J.L. Integrated state of subgenomic fragments of hepatitis B virus DNA in hepatocellular carcinoma from mainland China. *J. Natl. Cancer Inst.* **79**, 223–231 (1987).
30. Gozuacik, D. *et al.* Identification of human cancer-related genes by naturally occurring Hepatitis B Virus DNA tagging. *Oncogene* **20**, 6233–6240 (2001).
31. Puente, X.S. *et al.* Whole-genome sequencing identifies recurrent mutations in chronic lymphocytic leukaemia. *Nature* **475**, 101–105 (2011).
32. Qin, J., Jones, R.C. & Ramakrishnan, R. Studying copy number variations using a nanofluidic platform. *Nucleic Acids Res.* **36**, e116 (2008).


doi:10.1038/ng.2291

Antiviral Research 96 (2012) 59–64

Contents lists available at SciVerse ScienceDirect

Antiviral Research

journal homepage: www.elsevier.com/locate/antiviral

# Strong and multi-antigen specific immunity by hepatitis B core antigen (HBcAg)-based vaccines in a murine model of chronic hepatitis B: HBcAg is a candidate for a therapeutic vaccine against hepatitis B virus

Sheikh Mohammad Fazle Akbar [a,*], Shiyi Chen [b], Mamun Al-Mahtab [c], Masanori Abe [b], Yoichi Hiasa [b], Morikazu Onji [b]

[a] Department of Medical Sciences, Toshiba General Hospital, Higashi Oi 6-3-22, Shinagawa, Tokyo 140-8522, Japan
[b] Department of Gastroenterology and Metabology, Ehime University Graduate School of Medicine, Ehime, Toon City, Ehime 791-0295, Japan
[c] Department of Hepatology, Bangabandhu Sheikh Mujib Medical University, Shahbagh, Dhaka 1000, Bangladesh

ARTICLE INFO

*Article history:*
Received 11 April 2012
Revised 24 July 2012
Accepted 24 July 2012
Available online 1 August 2012

*Keywords:*
Chronic hepatitis B
Immune therapy
Hepatitis B core antigen
Dendritic cells

ABSTRACT

Experimental evidence suggests that hepatitis B core antigen (HBcAg)-specific cytotoxic T lymphocytes (CTL) are essential for the control of hepatitis B virus (HBV) replication and prevention of liver damage in patients with chronic hepatitis B (CHB). However, most immune therapeutic approaches in CHB patients have been accomplished with hepatitis B surface antigen (HBsAg)-based prophylactic vaccines with unsatisfactory clinical outcomes. In this study, we prepared HBsAg-pulsed dendritic cells (DC) and HBcAg-pulsed DC by culturing spleen DC from HBV transgenic mice (HBV TM) and evaluated the immunomodulatory capabilities of these antigens, which may serve as a better therapy for CHB. The kinetics of HBsAg, antibody levels against HBsAg (anti-HBs), proliferation of HBsAg- and HBcAg-specific lymphocytes, production of antigen-specific CTL, and activation of endogenous DC were compared between HBV TM vaccinated with either HBsAg- or HBcAg-pulsed DC. Vaccination with HBsAg-pulsed DC induced HBsAg-specific immunity, but failed to induce HBcAg-specific immunity in HBV TM. However, immunization of HBV TM with HBcAg-pulsed DC resulted in: (1) HBsAg negativity, (2) production of anti-HBs, and (3) development of HBsAg- and HBcAg-specific T cells and CTL in the spleen and the liver. Additionally, significantly higher levels of activated endogenous DC were detected in HBV TM immunized with HBcAg-pulsed DC compared to HBsAg-pulsed DC ($p < 0.05$). The capacity of HBcAg to modulate both HBsAg- and HBcAg-specific immunity in HBV TM, and activation of endogenous DC in HBV TM without inducing liver damage suggests that HBcAg should be an integral component of the therapeutic vaccine against CHB.



## 1. Introduction

Despite the considerable information regarding the viral life cycle, epidemiology, immunology, pathogenesis and prevention of hepatitis B virus (HBV), there has been a lack of significant developments in treating patients with chronic hepatitis B (CHB). Several antiviral drugs have been developed for treating CHB patients during the last three decades. However, controversy remains about their therapeutic efficacy. A systemic review of the National Institutes of Health (NIH) Consensus Development Conference, which assessed all randomized clinical trials on antiviral drugs in CHB patients from 1989 to 2008, revealed that antiviral drug treatment did not improve the clinical outcomes and all intermediate outcomes in CHB patients in any credible randomized-controlled trial (Shamliyan et al., 2009; Wilt et al., 2008). However, others have shown that these drugs could block or delay the progression of liver disease in CHB patients (Liaw, 2009; Lin et al., 1999). Although it is difficult to determine the underlying causes of these discrepancies, as different investigators used different criteria in their therapeutic evaluations, it is generally accepted that an ongoing treatment regimen for CHB with antiviral drugs is not satisfactory, and has low efficacy and considerable adverse effects. In addition, it is now clear that antiviral drugs possess poor immunomodulatory capabilities, which may be responsible for their ineffective control of HBV replication and inadequate prevention of liver damage in CHB (Lok and McMahon, 2007; Liaw and Chu, 2009).

* Corresponding author. Tel.: +81 3 3764 0511; fax: +81 3 3764 8992.
*E-mail addresses:* sheikh.akbar@po.toshiba.co.jp (S.M.F. Akbar), shiyi.chen.cn@gmail.com (S. Chen), shwapnil@agni.com (M. Al-Mahtab), masaben@m.ehime-u.ac.jp (M. Abe), hiasa@m.ehime-u.ac.jp (Y. Hiasa), onjimori@m.ehime-u.ac.jp (M. Onji).

0166-3542/$ - see front matter © 2012 Elsevier B.V. All rights reserved.
http://dx.doi.org/10.1016/j.antiviral.2012.07.011

Clinical and experimental evidence suggests that the replication of HBV DNA and progression of liver damage is under control in many CHB patients, even those not receiving any antiviral drug therapy. The magnitude and nature of host immunity to HBV is important in regulating these pathological events in CHB. In support of this concept, Maini et al. (2000) demonstrated that CHB patients that are capable of controlling HBV replication and liver damage harbor higher frequencies of hepatitis B surface antigen (HBsAg) and hepatitis B core antigen (HBcAg)-specific cytotoxic T lymphocytes (CTL) compared to those that express high levels of HBV and have progressive liver damage. Taken together, it appears that the restoration of host immune responses to HBV-related antigens may have therapeutic implications in CHB patients.

Based on these observations, polyclonal immunomodulators, such as cytokines, growth factors, and other immune mediators, were used in CHB patients. However, they had limited therapeutic efficacy and considerable side effects in CHB patients (Sprengers and Janssen, 2005). Subsequently, an antigen-specific immunotherapeutic approach, or vaccine therapy, was developed for CHB patients, which used commercially available prophylactic hepatitis B (HB) vaccines for treating CHB patients. Different investigators used different types of vaccines with different immunization protocols, and thus, it is difficult to assess the real therapeutic implications of vaccine therapy in CHB patients (Wang et al., 2010; Hoa et al., 2009; Pol et al., 2001). Indeed, it appears that the HBsAg-based vaccine may not be an effective immunotherapeutic approach in CHB. A well-planned clinical trial in 80 patients with CHB used a HBsAg-based vaccine in combination with another antiviral drug also failed to exhibit substantial therapeutic effect (Vandepapelière et al., 2007). Conversely, Heathcote et al. (1999) used a HBcAg epitope-based vaccine in CHB patients and achieved moderate therapeutic effects. Recently, Luo et al. (2010) reported that antigen-pulsed dendritic cells (DC) containing epitope of HBsAg and HBcAg had therapeutic effects in hepatitis B e antigen (HBeAg)-negative patients, but not in HBeAg-positive patients.

These clinical trials with HBsAg- and HBcAg-based vaccines have raised more questions than solutions regarding immune therapy for CHB patients, as the mechanisms of action of HBsAg- or HBcAg-based vaccine in CHB have not yet been explored. However, most cellular and molecular events following vaccination with either HBsAg or HBcAg could not be evaluated in CHB patients due to ethics, safety, technical, and procedural limitations.

To develop proper insights about immunogenecity of HBsAg- or HBcAg-based therapeutic vaccines in CHB, the role of DC in adaptive immunity has been examined. DC, the most potent antigen-presenting cells, are responsible for processing and presenting antigens for induction of antigen-specific immune responses in normal conditions as well as in the immune tolerance state (Steinman and Banchereau, 2007). Studies have shown that the phenotypes and functions of DC are distorted in chronic HBV infections (van der Molen et al., 2004). One way to circumvent immune tolerance state is to produce antigen-pulsed DC and use them as a vaccine. In fact, cancer antigen-pulsed DC and HBsAg-pulsed DC have been used to induce cancer-specific immunity and HBsAg-specific immunity in cancer patients and CHB patients, respectively, when antigen-specific immune responses could not be properly induced by only cancer antigen or HBsAg (Banchereau and Palucka, 2005; Steinman and Banchereau, 2007; Akbar et al., 2010a).

The present preclinical study assessed the immunomodulatory mechanisms of HBsAg and HBcAg in a murine model of HBV, specifically HBV transgenic mice (TM). After immunizing HBV TM with antigen-pulsed DC, the immune responses of HBsAg-pulsed DC or HBcAg-pulsed DC were compared in the spleen and liver. This study may provide further insight into developing an immune therapy for CHB patients.

## 2. Methods

### 2.1. Mice

HBV TM (official designation, 1.2HB-BS10) were prepared by microinjecting the complete genome of HBV plus 619 bp of HBV DNA into the fertilized eggs of C57BL/6 mice. HBV TM are known to express HBV DNA and mRNAs of 3.5, 2.1, and 0.8 kbp of HBV in the liver (Araki et al., 1989). HBV DNA were also detected in the liver, and HBsAg was found in the sera of all HBV TM. Eight-week-old male C57BL/6 mice were purchased from Nihon Clea (Tokyo, Japan). Mice were housed in polycarbonate cages in our laboratory facilities, and maintained in a temperature- and humidity-controlled room (23 ± 1 °C) with a 12-h light/dark cycle. All mice received humane care, and the study protocol was approved by the Ethics Committee of the Graduate School of Medicine, Ehime University, Japan. Eight-week-old C3H/He mice (Nihon Clea) were used in an allogenic mixed leukocyte reaction (MLR).

### 2.2. Detection of HBV-related markers

HBsAg levels and antibodies against HBsAg (anti-HBs) in sera were estimated with a chemiluminescence enzyme immunoassay (Special Reference Laboratory, Tokyo, Japan) and expressed as IU/ml and mIU/ml, respectively, as previously described (Akbar et al., 2010b).

### 2.3. Isolation of T lymphocytes, B lymphocytes, and DC

We have previously described in detail the methodology for isolating spleen cells and liver nonparenchymal cells (NPCs) (Akbar et al., 2010b; Chen et al., 2011; Yoshida et al., 2010). To produce a single cell suspension from the spleen, spleens were cut into pieces and passed through a 40-μm-pore nylon filter (BD Falcon, Durham, NC, USA). The resulting cells were collected and suspended in culture medium containing RPMI 1640 (Iwaki, Osaka, Japan) with 10% fetal calf serum (Filtron PTY Ltd., Brooklyn, Australia).

To retrieve liver NPCs, liver tissues were cut into pieces, homogenized, passed through 70-μm-pore steel meshes (Morimoto Yakuhin Co., Matsuyama, Japan), and suspended in 35% percoll (Sigma Chemical, St. Louis, MO, USA). After centrifugation for 15 min at 450 × *g* at room temperature, a high-density cell pellet was collected and suspended in culture medium.

T lymphocytes were isolated from the spleen single cell suspension or liver NPC by a negative selection column method using a mouse pan T isolation kit (Miltenyi Biotec, Bergish Gladbach, Germany), according to the manufacturer's directions (Chen et al., 2011; Yoshida et al., 2010).

DC were isolated from single cell suspensions of spleen and liver NPC using a density column (specific gravity 1.082), plastic adherence, re-culturing on plastic surface, and depletion of macrophages and lymphocytes or via positive selection of $CD11c^+$ cells with flow cytometry, as described (Akbar et al., 2010b, Chen et al., 2011).

### 2.4. Preparation of antigen-pulsed DC for immunizing HBV TM

HBsAg and HBcAg were purchased from Tokyo Institute of Immunology (Tokyo, Japan). Murine antigen-pulsed DC were prepared based on data from preliminary studies and according to our previous report (Akbar et al., 2010b; Miyake et al., 2010). Briefly, spleen DC were cultured with phosphate buffered solution (PBS) (unpulsed DC) or pyruvate dehydrogenase complex (PDC,

Sigma Biochemical, St. Louis, MO, USA) or HBsAg or HBcAg in culture medium for 48 h. DC were recovered from the cultures and washed five times with PBS. The viability of DC was assessed with a trypan blue exclusion test. The production of cytokines and T cell stimulatory capacities of antigen-pulsed DC were assessed *in vitro*.

### 2.5. Immunization schedule

HBV TM with comparable sera levels of HBsAg were used for this study. HBV TM were injected with either $5 \times 10^6$ unpulsed DC or $5 \times 10^6$ PDC-pulsed DC or $5 \times 10^6$ HBsAg-pulsed DC, or $5 \times 10^6$ HBcAg-pulsed DC. All vaccinations were done via the intraperitoneal route, six times, at an interval of 2 weeks. HBV TM were bled from the tail vein at different time intervals for assessments of various immunological parameters. HBV TM were sacrificed at different times after the initiation of immunization to estimate vaccine-induced cellular immune responses in the spleen and liver.

### 2.6. Lymphoproliferative assays

As described previously, murine lymphocytes were cultured in the absence or presence of different antigens to evaluate antigen-specific cellular immune responses (Akbar et al., 2010b; Chen et al., 2011; Yoshida et al., 2010). All cultures were performed in 96-well U-bottom plates (Corning Incorporated, New York, NY, USA). $^3$H-thymidine (1.0 μCi/ml, Amersham Biosciences, Little Chalfont, Buckinghamshire, UK) was diluted in sterile PBS, added to the cultures for the last 16 h, and harvested automatically via a multiple cell harvester (LABO MASH, Futaba Medical, Osaka, Japan) onto filter paper (LM 101–10, Futaba Medical). [$^3$H]-thymidine levels of incorporation were determined with a liquid scintillation counter (Beckman LS 6500, Beckman Instruments, Inc., Fullerton, CA, USA) at blastogenesis. Triplicate cultures were assayed routinely and the results were expressed as counts per minute (cpm). The stimulation index was calculated as the ratio of cpm obtained in the presence of antigen or antigen-pulsed DC to that obtained without antigen or in presence of only DC or irrelevant antigen-pulsed DC (i.e., control culture). A stimulation index >3.0 was considered significant.

### 2.7. ELISPOT assay

CD8$^+$ T lymphocytes ($1 \times 10^5$) were stimulated with the antigen in presence of mitomycin C-treated spleen adherent cells in an IFN-γ coated ELISPOT plate (Mabtech, Nacka Strand, Sweden) for 24 h (Akbar et al., 2010a; Yoshida et al., 2010). Subsequently, biotinylated antibodies (2A5-biotin, Mabtech) were added into the wells. After 2 h of incubation, the plates were incubated with streptavidin–alkaline phosphatase for 1 h. After washing the plates, the substrate solution, BCIP/NBT, was added. The reaction was stopped by washing the plates extensively with tap water. The numbers of spot-forming units (SFU) were counted using an ELISPOT reader (KS ELISPOT, Carl Zeiss, Thornwood, NY, USA), and subtracted from the numbers of background SFU of control wells.

### 2.8. Estimation of cytokine levels

Various cytokine levels were estimated in culture supernatants using a commercial kit for the cytometric bead array method, as previously described (Akbar et al., 2010b; Yoshida et al., 2010). Cytokines levels were calibrated to the mean fluorescence intensities of the standard negative control, standard positive control, and samples with Cytometric Bead Array software (BD Biosciences Pharmingen, San Jose, CA, USA) on a Macintosh computer (SAS Institute, Cary, NC, USA).

### 2.9. Statistical analysis

Data are shown as mean ± standard deviation (SD). Differences were compared using the Student's *t* test. For differences determined by the *F* test, the *t* test was adjusted for unequal variances (Mann–Whitney's *U*-test). $p < 0.05$ was considered statistically significant.

## 3. Results

### 3.1. Evaluation of specificity of the experimental system

To assess the specificity of the experimental system, we immunized normal C57BL/6 mice twice with 10 μg of HBsAg or 10 μg of HBcAg, or 10 μg of PDC to induce antigen-specific lymphocytes in normal mice. Antigen-pulsed DC were prepared by culturing spleen DC from normal C57BL/6 mice with different antigens. HBsAg-, HBcAg-, and PDC-pulsed DC induced significant lymphoproliferation in mice immunized with HBsAg-, HBcAg-, and PDC, respectively. However, HBsAg-specific lymphoproliferation was not detected in mice immunized with HBcAg-pulsed DC or PDC-pulsed DC. Additionally, HBcAg and PDC-specific lymphocytes could not be retrieved from mice immunized with non-relevant antigens (Table 1). HBcAg-pulsed DC induced significantly higher levels of antigen-specific lymphoproliferation compared to HBsAg-pulsed DC (stimulation index, 31 ± 5 versus 15 ± 3.2, $N = 5$, $p < 0.05$) (Table 1).

After assessing the immunogenecity of antigen-pulsed DC of normal C57BL/6 mice *in vitro*, we prepared antigen-pulsed DC from HBV TM. Antigen-pulsed DC from HBV TM produced significantly higher levels of IFN-γ and IL-12 compared to unpulsed DC ($p < 0.05$). They also induced antigen-specific lymphoproliferation in normal mice immunized with the respective antigens (data not shown).

### 3.2. HBsAg negativity and anti-HBs production by antigen-pulsed DC

To assess if antigen-pulsed DC were capable of inducing HBsAg negativity and anti-HBs production in HBV TM, we checked HBsAg and anti-HBs in these mice at different times after vaccinations. HBsAg and anti-HBs levels were assessed in the sera of HBV TM before (0), and after 2, 4, and 6 vaccinations with various combinations of antigen-pulsed DC. All HBV TM expressed HBsAg in the sera, and anti-HBs were not detected in any of the mice prior to vaccination. In each group, 15 HBV TM were included for analyses.

Immunization of HBV TM with unpulsed DC or PDC-pulsed DC did not result in significant alteration in serum HBsAg levels.

**Table 1**
Antigen-specific proliferation of T cells by antigen-pulsed dendritic cells.

| Lymphocytes | Dendritic cells (DC) | Stimulation index |
|---|---|---|
| HBsAg-immunized mice | PDC-pulsed DC | 1.0 |
| | HBsAg-pulsed DC | 15 ± 3.2* |
| | HBcAg-pulsed DC | 1.7 ± 0.5 |
| HBcAg-immunized mice | PDC-pulsed DC | 1.0 |
| | HBsAg-pulsed DC | 1.9 ± 0.5 |
| | HBcAg-pulsed DC | 31 ± 5.2* |
| PDC-immunized mice | HBsAg-pulsed DC | 1.0 |
| | HBcAg-pulsed DC | 1.8 ± 0.6 |
| | PDC-pulsed DC | 9.2 ± 2* |

Normal C57BL/6J mice were immunized with HBsAg, HBcAg, and PDC. Antigen-pulsed DC were prepared by culturing DC with different antigens, as described in the Section 2. Mice were sacrificed 4 weeks after the second immunization, and spleen cells were stimulated with different types of DC. The levels of blastogenesis in cultures containing T cells and irrelevant antigen-pulsed DC were regarded to as a stimulation index of 1.0. Data are presented as mean and standard deviation of five separate experiments. Stimulation index > 3.0 was regarded to as significant antigen-specific proliferation. *<0.05 vs.T cells stimulated with irrelevant antigen-pulsed DC.

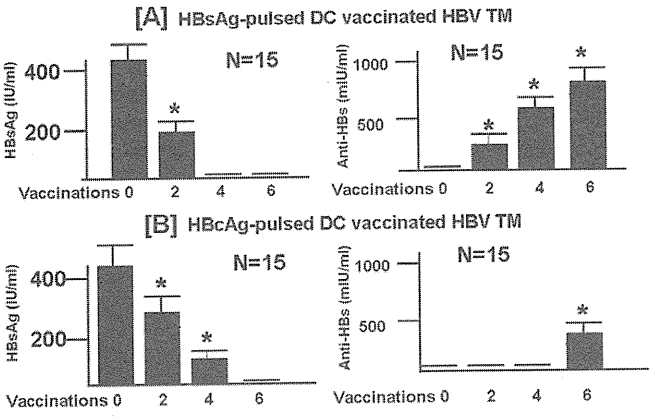


**Fig. 1.** HBsAg negativity and development of anti-HBs in HBV TM immunized with (a) HBsAg-pulsed DC ($n = 15$) and (B) HBcAg-pulsed DC ($n = 15$). HBsAg and anti-HBs were estimated in the sera by chemiluminescence enzyme immunoassay and expressed as IU/ml and mIU/ml, respectively. Data are presented as mean and standard deviation. 0, 2, 4, and 6 represent before vaccination, after two vaccinations, after four vaccinations and after six vaccinations, respectively. $^{*}p < 0.05$ compared to before vaccination (0).

Additionally, anti-HBs were not detected in HBV TM immunized with unpulsed DC and PDC-pulsed DC (data not shown).

HBsAg and anti-HBs levels at different time points after administration of antigen-pulsed DC are presented in Fig. 1. Eight of the 15 HBV TM immunized with HBsAg-pulsed DC became negative for HBsAg after two vaccinations, and all HBV TM became negative for HBsAg after four vaccinations. High levels of anti-HBs were induced in HBV TM after six vaccinations with HBAg-pulsed DC (Fig. 1A).

Interestingly, immunization with HBcAg-pulsed DC also resulted in a downregulation of HBsAg in HBV TM. All HBV TM immunized with HBcAg-pulsed DC became negative for HBsAg after six vaccinations. Anti-HBs were also detected in all HBV TM immunized with six vaccinations with HBcAg-pulsed DC (Fig. 1B).

### 3.3. Proliferation of antigen-specific spleen T lymphocytes in HBV TM due to immunization with antigen-pulsed DC

In order to develop insights about role of antigen-pulsed DC on proliferative responses of T lymphocytes, *in vitro* studies were accomplished with spleen T lymphocytes of HBV TM. Six vaccinations with unpulsed DC or PDC-pulsed DC did not induce HBsAg- and HBcAg-specific lymphocytes in HBV TM, as the spleen T lymphocytes of these mice did not show significant proliferation following stimulation with HBsAg or HBcAg *in vitro* (data not shown).

Antigen-specific proliferation of spleen T lymphocytes in HBV TM immunized with HBsAg-pulsed DC is presented in Table 2, panel A. The proliferation levels of T lymphocytes before vaccination were considered a stimulation index of 1.0. T lymphocytes from the spleen of HBV TM immunized with HBsAg-pulsed DC exhibited significant T cell proliferative responses to HBsAg (stimulation index 17.4 ± 4.3, $n = 5$). However, T lymphocytes of HBV TM immunized with HBsAg-pulsed DC did not demonstrate any HBcAg-specific immune responses (Table 1, panel A). Conversely, spleen T lymphocytes from HBV TM immunized with HBcAg-pulsed DC showed significant levels of proliferation in response to both HBsAg (stimulation index, 28.4 ± 3.8, $N = 5$) and HBcAg (stimulation index, 41.2 ± 4.1, $N = 5$).

### 3.4. Immunization of HBV TM with HBcAg-pulsed DC induced HBcAg- and HBsAg-specific IFN-γ producing $CD8^+$ cytotoxic T lymphocytes (CTL) in the liver

To compare the capacities of HBsAg-pulsed DC or HBcAg-pulsed DC to induce antigen-specific immune responses in the liver of HBV TM, HBsAg-specific and HBcAg-specific CTL were enumerated among liver NPC. Immunization of HBV TM with unpulsed DC or PDC-pulsed DC did not induce significant numbers of CTL (i.e., IFN-γ producing $CD8^+$ T) in the liver following stimulation with HBsAg or HBcAg. Considerable numbers of CTL were detected among liver $CD8^+$ T lymphocytes of HBV TM immunized with HBsAg-pulsed DC following stimulation with HBsAg *in vitro* (213 ± 23, $N = 5$) but not with HBcAg (17 ± 6, $N = 5$) (Table 2, panel B). Conversely, very high proportions of both HBcAg-specific $CD8^+$ CTL (623 ± 38, $N = 5$) and HBsAg-specific $CD8^+$ CTL (453 ± 32, $N = 5$) were detected in the liver of HBV TM immunized with HBcAg-pulsed DC (Table 2, panel B).

**Table 2**
Antigen-specific T cells in the spleen and the liver of HBV TM immunized with antigen-pulsed DC.

| HBV TM immunized with | HBsAg-specific T cell proliferation | HBcAg-specific T cells proliferation |
|---|---|---|
| (A) *Antigen-specific T cells in the spleen of HBV TM immunized with antigen-pulsed DC* | | |
| HBsAg-pulsed DC | 17.4 ± 4.3 | 1.2 ± 0.4 |
| HBcAg-pulsed DC | 28.4 ± 3.8 | 41.2 ± 4.1 |
| HBV TM immunized with | HBsAg-specific ELISPOT | HBcAg-specific ELISPOT |
| (B) *IFN-γ-secreting CD8 + T-cells in the liver of HBV TM immunized with antigen-pulsed DC* | | |
| Unpulsed DC | 13 ± 4 | 11 ± 3 |
| PDC pulsed DC | 13 ± 3 | 12 ± 3 |
| HBsAg-pulsed DC | 213 ± 23* | 17 ± 6 |
| HBcAg-pulsed DC | 453 ± 32* | 623 ± 38* |

Hepatitis B virus (HBV) transgenic mice (TM) were injected with unpulsed DC, pyruvate dehydrogenase complex (PDC)-pulsed DC, hepatitis B surface antigen (HBsAg)-pulsed DC, or hepatitis B core antigen (HBcAg)-pulsed DC, six times every 2 weeks. HBV TM were sacrificed 2 weeks after the last vaccination.
Panel A: Spleen T cells were evaluated for antigen-specific proliferation in lymphoproliferative assay. The proliferation levels of T lymphocytes before vaccination were regarded as stimulation index of 1.0. Data are presented as mean and standard deviation of five separate experiments.
Panel B: Liver $CD8^+$ T cells were stimulated with HBsAg or HBcAg on an ELISPOT plate to assay IFN-γ production. Data are presented as mean and standard deviation of five separate experiments. *<0.05 vs. HBV TM immunized with unpulsed DC or PDC-pulsed DC.

### 3.5. Increased production of proinflammatory cytokines by liver NPC from HBV TM immunized with HBcAg-pulsed DC compared to those immunized with HBsAg-pulsed DC

To evaluate cytokine production by liver NPC from HBV TM immunized with HBsAg-pulsed DC or HBcAg-pulsed DC, Liver NPC from HBV TM immunized with HBsAg- or HBcAg-pulsed DC were cultured with HBsAg or HBcAg. IFN-γ and TNF-α levels were significantly higher in HBV TM immunized with HBsAg- or HBcAg-pulsed DC compared to unpulsed HBV TM ($p < 0.05$) (Fig. 2). However, the levels of both cytokines were significantly higher in HBV TM immunized with HBcAg-pulsed DC compared to those immunized with HBsAg-pulsed DC ($p < 0.05$) (Fig. 2).

### 3.6. Increased activation of endogenous DC via administration of HBcAg-pulsed DC in HBV TM

Although antigen-pulsed DC induced antigen-specific T lymphocytes in HBV TM, it was necessary to assess if antigen-pulsed DC can activate endogenous DC of these mice. Four weeks after six vaccinations with antigen-pulsed DC in HBV TM, DC were isolated from HBV TM to assess the functional capacities of endogenous DC. DC were cultured with allogenic T lymphocytes from

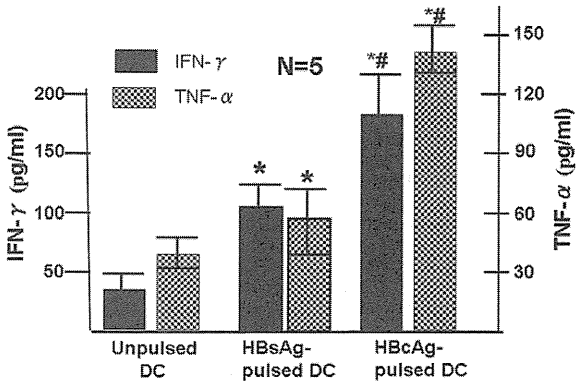


**Fig. 2.** Significantly higher levels of IFN-γ and TNF-α production via liver NPC in HBV TM immunized with HBcAg-pulsed DC compared to those immunized with HBsAg-pulsed DC. Liver NPC from HBV TM immunized with unpulsed DC or HBsAg-pulsed DC or HBcAg-pulsed DC were cultured with HBsAg or HBcAg and the levels of IFN-γ and TNF-α were estimated by CBA method. Mean and standard deviation of IFN-γ (black bar) and TNF-α (checkered bar) levels produced via liver NPC following immunization with unpulsed DC, HBsAg-pulsed DC, and HBcAg-pulsed DC in five separate experiments. $^{*}p < 0.05$ vs. HBV TM immunized with unpulsed DC. $^{\#}p < 0.05$ vs. HBV TM immunized with HBsAg-pulsed DC.

C3H/He mice, and T cell proliferation levels in allogenic MLR and cytokines in culture supernatants were estimated. The allostimulatory capacities of DC were significantly higher in HBV TM immunized with HBsAg- or HBcAg-pulsed DC compared to DC from HBV TM immunized with unpulsed DC (Fig. 3). HBV TM immunized with HBcAg-pulsed DC showed significantly higher T cell proliferation levels than DC from HBV TM immunized with HBsAg-pulsed DC (Fig. 3A).

As shown in Fig. 3B, IFN-γ and TNF-α levels were also significantly higher in culture supernatants of allogenic MLR containing DC from HBV TM immunized with HBsAg- or HBcAg-pulsed DC compared to those containing DC from HBV TM immunized with unpulsed DC ($p < 0.05$). The levels of IFN-γ were significantly higher in cultures containing DC from HBcAg-pulsed immunized HBV TM compared to HBsAg-pulsed immunized HBV TM ($p < 0.05$).

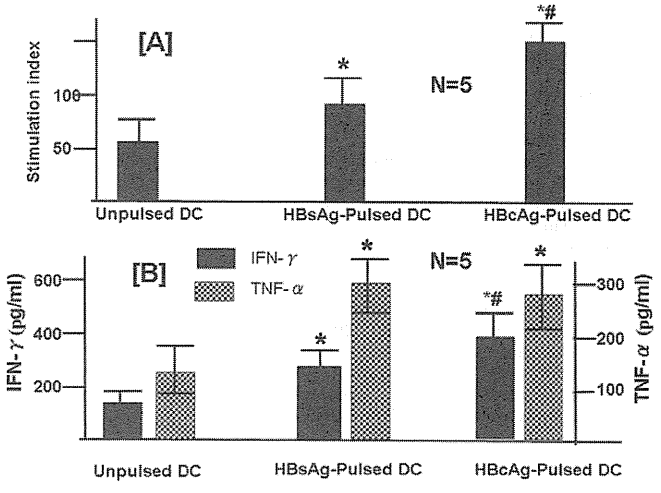


**Fig. 3.** Increased immunogenicity of DC in HBV TM immunized with HBcAg-pulsed DC compared to HBV TM immunized with HBsAg-pulsed DC. DC were cultured with allogenic T lymphocytes from C3H/He mice, and T cell proliferation levels in allogenic MLR and cytokines in culture supernatants were estimated. (A) Allostimulatory capacity of DC from HBV TM immunized with unpulsed DC or HBsAg-pulsed DC or HBcAg-pulsed DC. (B) Production of IFN-γ (Black bar) and TNF-α (checkered bar) in culture containing DC from HBV TM immunized with unpulsed DC or HBsAg-pulsed DC, or HBcAg-pulsed DC. Data are presented as mean and standard deviation of the stimulation index and cytokines in five separate experiments. $^{*}p < 0.05$ vs. HBV TM immunized with unpulsed DC. $^{\#}p < 0.05$ vs. HBV TM immunized with HBsAg-pulsed DC.

## 4. Discussion

Antigen-based immune therapy (vaccine therapy) has emerged as a potential therapeutic approach for CHB patients, as it is based on the concept of controlling HBV replication and preventing liver damage in CHB by inducing and maintaining HBV-specific immune responses. Investigators have shown that non HBV-specific immune responses are mainly responsible for impaired control of HBV replication and progressive liver damages in CHB patients, whereas, HBV-specific immune responses, especially HBcAg-specific CTL, are related to control of HBV replication and containment of liver damages in CHB patients (Bertoletti and Maini, 2000). CHB patients that are capable of controlling HBV replication and liver damage harbor higher frequencies of HBV-specific immunocytes, especially HBcAg-specific CTL, compared to those that express high levels of HBV and have progressive liver damage (Maini et al., 2000). These facts show that vaccine therapy can be regarded as an evidence-based therapeutic approach for CHB patients, however, there is still controversy regarding the therapeutic strategies of using vaccines. Although several variables may be important in this context, such as the nature of the antigen, dose of antigen, duration of therapy, and nature of adjuvant, it is of utmost importance to develop further insight regarding the nature of antigens that are proposed to be used as therapeutic vaccines in CHB. After the first clinical trial on HBsAg-based vaccine therapy conducted by Pol et al. (1994), several studies during the last 15 years have pointed to the inherent limitations of HBsAg-based vaccines, even if these therapies are given in combination with antiviral drugs (Pol et al., 2001; Vandepapelière et al., 2007) or loaded on DC or other immunocytes (Akbar et al., 2010a). Both Hoa et al. (2009) and Akbar et al. (2010a) found that HBsAg-based vaccine therapy induced HBsAg-specific immunity and anti-HBs in some CHB patients, but these were not translated into therapeutic efficacy, as adequate levels of HBcAg-specific immunity was not induced.

The data from these studies suggests that HBcAg-pulsed DC are capable of: (1) inducing HBsAg negativity in the sera, (2) developing anti-HBs in the sera, and (3) inducing both HBsAg and HBcAg-specific T cells and CTL in the spleen and the liver. The induction of HBcAg-specific immunity was expected in HBV TM immunized with HBcAg-pulsed DC. However, the effects of HBcAg-pulsed DC on HBsAg-specific immunity in HBV TM is worthy of consideration in the context of immune therapy. Our data corroborates previous reports on the wide-spread immunomodulatory capacities of HBcAg as an adjuvant to HBsAg-specific immunity (Lobaina et al., 2005; Aguilar et al., 2004).

In the present study, we also explored the mechanisms underlying the immunomodulatory effects of HBcAg. It was found that the strong immunomodulatory capabilities of HBcAg may be due to an establishment of an inflammatory hepatic microenvironment, induction of HBcAg-specific CTL in the liver, and activation of host DC. Lee et al. (2009) has reported that HBcAg activates innate immunity. Although we have not checked activation levels of cells of innate immunity in this study, increased production of pro-inflammatory cytokines by liver NPC of HBV TM immunized with HBcAg-pulsed DC compared to those immunized with HBsAg-pulsed DC provide an indirect support for the notion that innate immunity may be stimulated by HBcAg. However, this remains to be confirmed in future in more details.

Taken together, HBcAg should be an integral part of a therapeutic vaccine against chronic HBV infection. However, factors, such as the dose of antigen and duration of therapy, should be properly determined prior to the development of therapeutic vaccines

against CHB. In a previous report (Akbar et al., 2010b), we could not induce HBsAg-specific immune responses by HBcAg-based immunization by loading spleen DC with 10 μg of HBcAg and administrating 2 million DC twice. In this study, we loaded DC with 50 μg of HBcAg and administered 5 million HBcAg-pulsed DC six times. Thus, additional studies would be required to determine the influence of factors, such as dose and duration of therapy, in restoring immunity in CHB.

The clinical utility of the data presented herein may not be translatable to the human condition, as there are fundamental differences between HBV TM and CHB patients. In addition, HBV TM do not demonstrate all of the different features of HBV-related pathogenesis, as they have no evidence of liver injury and exhibit very low levels or almost no circulating HBV DNA. Thus, the implications of these findings need to be confirmed in CHB patients, and the role of HBcAg should be further assessed in humans. The major limitation of the present study lies in the fact that human consumable and commercially developed HBcAg are seldom available for clinical trials in human. To address this issue, we have been conducting a clinical trial with a human consumable HBcAg/HBsAg conjugate vaccine in CHB patients. Preliminary outcomes suggest that the HBsAg/HBcAg-based vaccine induces HBV negativity in 50% of subjects, diminishes liver damage in almost all of the patients, and induces HBsAg- and HBcAg-specific immune responses (Akbar et al., 2010c). However, the relative contribution of HBsAg and HBcAg in this protocol could not be assessed properly. A future study has been designed in which only human consumable HBcAg will be used as a therapeutic vaccine in CHB.

It is still unclear whether HBcAg-based or a conjugate vaccine containing both HBcAg and HBsAg may be required in the design of an evidence-based immunotherapeutic approach against CHB. The findings of the present study, as well as the clinical observations with the HBcAg/HBsAg-based vaccine (Akbar et al., 2010c) in CHB, indicate that HBcAg should be an integral part of a therapeutic vaccine against CHB.

## References


Aguilar, J.C., Lobaina, Y., Muzio, V., García, D., Pentón, E., Iglesias, E., Pichardo, D., Urquiza, D., Rodríguez, D., Silva, D., Petrovsky, N., Guillén, G., 2004. Development of a nasal vaccine for chronic hepatitis B infection that uses the ability of hepatitis B core antigen to stimulate a strong Th1 response against hepatitis B surface antigen. Immunol. Cell. Biol. 82, 539–546.

Akbar, S.M., Furukawa, S., Horiike, N., Abe, M., Hiasa, Y., Onji, M., 2010a. Safety and immunogenecity of hepatitis B surface antigen-pulsed dendritic cells in patients with chronic hepatitis B. J. Viral. Hepat. 18, 408–414.

Akbar, S.M., Yoshida, O., Chen, S., Aguilar, A.J., Abe, M., Matsuura, B., Hiasa, Y., Onji, M., 2010b. Immune modulator and antiviral potential of dendritic cells pulsed with both hepatitis B surface antigen and core antigen for treating chronic HBV infection. Antivir. Ther. 15, 887–895.

Akbar, S.M., Al-Mahtab, M., Rahman, S., Aguilar, J.C., Onji, M., Mishiro, S., 2010c. Therapeutic potential of a novel therapeutic vaccine containing both hepatitis B surface antigen (HBsAg) and hepatitis B core antigen (HBcAg) administered through mucosal and parental route in patients with chronic hepatitis B. Hepatology 52 (Suppl.), 438A–439A.

Araki, K., Miyazaki, J., Hino, O., Tomita, N., Chisaka, O., Matsubara, K., Yamamura, K., 1989. Expression and replication of hepatitis B virus genome in transgenic mice. Proc. Natl. Acad. Sci. USA 86, 207–211.

Banchereau, J., Palucka, A.K., 2005. Dendritic cells as therapeutic vaccines against cancer. Nat. Rev. Immunol. 5, 296–306.

Bertoletti, A., Maini, M.K., 2000. Protection or damage: a dual role for the virus-specific cytotoxic T lymphocyte response in hepatitis B and C infection? Curr. Opin. Microbiol. 3, 387–392.

Chen, S., Akbar, S.M., Abe, M., Hiasa, Y., Onji, M., 2011. Immunosuppressive functions of hepatic myeloid-derived suppressor cells of normal mice and in a murine model of chronic hepatitis B virus. Clin. Exp. Immunol. 166, 134–142.

Heathcote, J., McHutchison, J., Lee, S., Tong, M., Benner, K., Minuk, G., Wright, T., Fikes, J., Livingston, B., Sette, A., Chestnut, R.The CY1899 T Cell Vaccine Study Group, 1999. A pilot study of the CY-1899 T-cell vaccine in subjects chronically infected with hepatitis B virus. Hepatology 30, 531–536.

Hoa, P.T., Huy, N.T., Thu le, T., Nga, C.N., Nakao, K., Eguchi, K., Chi, N.H., Hoang, B.H., Hirayama, K., 2009. Randomized controlled study investigating viral suppression and serological response following pre-S1/pre-S2/S vaccine therapy combined with lamivudine treatment in HBeAg-positive patients with chronic hepatitis B. Antimicrob. Agents Chemother. 53, 5134–5140.

Lee, B.O., Tucker, A., Frelin, L., Sallberg, M., Jones, J., Peters, C., Hughes, J., Whitacre, D., Darsow, B., Peterson, D.L., Milich, D.R., 2009. Interaction of the hepatitis B core antigen and the innate immune system. J. Immunol. 182, 6670–6681.

Liaw, Y.F., 2009. Natural history of chronic hepatitis B virus infection and long-term outcome under treatment. Liver Int. 29 (Suppl 1), 100–107.

Liaw, Y.F., Chu, C.M., 2009. Hepatitis B virus infection. Lancet 373, 582–592.

Lin, S.M., Sheen, I.S., Chien, R.N., Chu, C.M., Liaw, Y.F., 1999. Long-term beneficial effect of interferon therapy in patients with chronic hepatitis B virus infection. Hepatology 29, 971–975.

Lobaina, Y., Palenzuela, D., Pichardo, D., Muzio, V., Guillén, G., Aguilar, J.C., 2005. Immunological characterization of two hepatitis B core antigen variants and their immunoenhancing effect on co-delivered hepatitis B surface antigen. Mol. Immunol. 42, 289–294.

Lok, A.S., McMahon, B.J., 2007. Chronic hepatitis B. Hepatology 45, 507–539.

Luo, J., Li, J., Chen, R.L., Nie, L., Huang, J., Liu, Z.W., Luo, L., Yan, X.J., 2010. Autologus dendritic cell vaccine for chronic hepatitis B carriers: a pilot, open label, clinical trial in human volunteers. Vaccine 28, 2497–2504.

Maini, M.K., Boni, C., Lee, C.K., Larrubia, J.R., Reignat, S., Ogg, G.S., King, A.S., Herberg, J., Gilson, R., Alisa, A., Williams, R., Vergani, D., Naoumov, N.V., Ferrari, C., Bertoletti, A., 2000. The role of virus-specific CD8(+) cells in liver damage and viral control during persistent hepatitis B virus infection. J. Exp. Med. 191, 1269–1280.

Miyake, T., Akbar, S.M., Yoshida, O., Chen, S., Hiasa, Y., Matsuura, B., Abe, M., Onji, M., 2010. Impaired dendritic cell functions disrupt antigen-specific adaptive immune responses in mice with non alcoholic fatty liver disease. J. Gastroenterol. 45, 859–867.

Pol, S., Driss, F., Michel, M.L., Nalpas, B., Berthelot, P., Brechot, C., 1994. Specific vaccine therapy in chronic hepatitis B infection. Lancet 344 (8918), 342.

Pol, S., Nalpas, B., Driss, F., Michel, M.L., Tiollais, P., Denis, J., Brécho, C., 2001. Multicenter study group. Efficacy and limitations of a specific immunotherapy in chronic hepatitis B. J. Hepatol. 34, 917–921.

Shamliyan, T.A., MacDonald, R., Shaukat, A., Taylor, B.C., Yuan, J.M., Johnson, J.R., Tacklind, J., Rutks, I., Kane, R.L., Wilt, T.J., 2009. Antiviral therapy for adults with chronic hepatitis B: A systemic review for a National Institute of Health consensus development conference. Ann. Intern. Med. 150, 111–124.

Sprengers, D., Janssen, H.L., 2005. Immunomodulatory therapy for chronic hepatitis B virus infection. Fund Clin. Pharmacol. 19, 17–26.

Steinman, R.M., Banchereau, J., 2007. Taking dendritic cells into medicine. Nature 449, 419–426.

van der Molen, R.G., Sprengers, D., Binda, R.S., de Jong, E.C., Niesters, H.G., Kusters, J.G., Kwekkeboom, J., Janssen, H.L., 2004. Functional impairment of myeloid and plasmacytoid dendritic cells of patients with chronic hepatitis B. Hepatology 40, 738–746.

Vandepapelière, P., Lau, G.K., Leroux-Roels, G., Horsmans, Y., Gane, E., Tawandee, T., Merican, M.I., Win, K.M., Trepo, C., Cooksley, G., Wettendorff, M., Ferrari, C., 2007. Therapeutic HBV Vaccine Group of Investigators. Therapeutic vaccination of chronic hepatitis B patients with virus suppression by antiviral therapy: a randomized, controlled study of co-administration of HBsAg/AS02 candidate vaccine and lamivudine. Vaccine 25, 8585–8597.

Wang, X.Y., Zhang, X.X., Yao, X., Jiang, J.H., Xie, Y.H., Yuan, Z.H., Wen, Y.M., 2010. Serum HBeAg sero-conversion correlated with decrease of HBsAg and HBV DNA in chronic hepatitis B patients treated with a therapeutic vaccine. Vaccine 28, 8169–8174.

Wilt, T.J., Shamliyan, T., Shaukat, A., Taylor, B.C., MacDonald, R., Yuan, J.M., Johnson, J.R., Tacklind, J., Rutks, I., Kane, R.L., 2008. Management of chronic hepatitis B. Evid. Rep. Technol. Assess (Full Rep.) 174, 1–671.

Yoshida, O., Akbar, S.M., Chen, S., Miyake, T., Abe, M., Hiasa, Y., Murakami, H., Onji, M., 2010. Regulatory natural killer cells in murine liver and their immunosuppressive capacity. Liver Int. 30, 906–912.